Shifts in phenology and species ranges synergistically alter the timing and species composition of the flowering season Authors: Tadeo H. Ramirez-Parada<sup>1</sup>, Isaac W. Park<sup>2</sup>, Shijia Peng<sup>3</sup>, Misako Nishino<sup>4</sup>, John T. Kartesz<sup>4</sup>, Sydne Record<sup>5</sup>, Charles C. Davis<sup>6</sup>, Susan J. Mazer<sup>1</sup>. Institutional Affiliations: <sup>1</sup>Department of Ecology, Evolution, and Marine Biology, University of California, Santa Barbara, CA 93106, USA. <sup>2</sup>Department of Biology, Georgia Southern University, Statesboro, GA 30460, USA. <sup>3</sup>Department of Earth Sciences, University of Oxford, Oxford OX1 3AN, UK. <sup>4</sup>Biota of North America Program (BONAP), Chapel Hill, 27516, North Carolina, USA <sup>5</sup>Department of Wildlife, Fisheries, and Conservation Biology, University of Maine, Orono, ME, 04469, USA. Department of Organismic and Evolutionary Biology, Harvard University, Cambridge, MA 02138, USA. Corresponding author: Tadeo H. Ramirez-Parada, tadeoramirezp@gmail.com 

## **Abstract**

19

20

21

22

23

24

25

26

27

28

29

30

31

32

33

34

35

36

37

38

39

40

Global change is altering the phenology and geographic ranges of flowering species, with potentially profound consequences for the timing and composition of floral resources and the seasonal structure of ecological communities. However, shifts in flowering phenology and species distributions have historically been studied in isolation due to disciplinary silos and limited data, leaving critical gaps in our understanding of their combined effects. To address this, we used millions of herbarium and occurrence records to model phenological and range shifts for 2,837 plant species in the United States across historical, recent, and projected climate and land cover conditions, enabling us to scale responses from species to communities, and from local to continental geographies. Our analysis reveals that communities are shifting toward earlier, longer flowering seasons in most biomes, with co-flowering species richness increasing at the edges of the season and declining at historical peaks—trends projected to intensify under ongoing environmental trends. Although range and phenology shifts operate concurrently, they predominantly affect different aspects of the flowering season: phenological changes primarily alter seasonality—its start, end, and duration—and co-flowering diversity at the edges of the season, while range shifts more strongly influence co-flowering species richness during historical seasonal peaks and the identity and degree of flowering synchrony among co-occurring species pairs. Together, these results demonstrate that shifts in phenology and species ranges act synergistically to restructure the flowering seasons across the conterminous United States, revealing wide variation in the pace and magnitude of change among biomes.

## Introduction

The start, end, duration, and species composition of a community's flowering season—the period during which most co-occurring angiosperms complete their annual flowering cycles within temperate communities—impacts the fitness of both plants and of organisms reliant on floral resources. These attributes mediate the seasonal distribution and diversity of flowering species within a community, which in turn influences pollinator population growth rates (Roulston & Goodell, 2011) and various density-dependent ecological outcomes in plants—such as competition, pollination, or florivory—that can impact their population persistence and the evolution of life-history strategies (Elzinga et al., 2007).

Recent climate and land use changes have led to widespread shifts in flowering phenology and in plant distributions (Cleland et al., 2007; Kelly & Goulden, 2008; Ramirez-Parada et al., 2024), often disrupting ecological interactions through altered spatial and seasonal synchrony between species (Renner & Zohner, 2018; Theobald et al., 2017). However, how species-level shifts in phenology and distributions scale to the community level to jointly affect the structure of the flowering season (e.g., its start, end, duration, and the seasonal distribution of co-flowering species richness) is poorly understood. This is largely because these processes have historically been studied separately (Parmesan & Hanley, 2015), but also because long-term datasets including enough species to characterize a community's flowering season are rare and often temporally and spatially limited (CaraDonna et al., 2014). Elucidating how shifts in phenology and species ranges affect the structure of the flowering season at the community level—and understanding how these effects are distributed across regions and biomes—is essential for forecasting the impacts of global change on terrestrial ecosystems.

Shifting phenology and species ranges should have distinct impacts on the start, end, duration, and species composition of the flowering season (henceforth 'the structure of the flowering season') because these processes differ in their degree of temporal structure (Fig. 1). For example, in the temperate zone, phenological responses to climate—which are primarily caused by phenotypic plasticity—tend to differ markedly among species flowering early and late in the season, with spring-flowering species advancing flowering in response to warming and late summer- and fall-flowering species typically showing limited responsiveness or flowering delays (D. S. Park et al., 2019; Ramirez-Parada et al., 2024). In contrast, changes in species

71 diversity typically impact the phenology of remaining species indirectly (e.g., through changes in soil nitrogen or moisture) (Wolf et al., 2017), and species lost or gained within most 72 73 communities do not tend to flower predominantly early or late within the season (but see 74 counterexamples among invasive species) (Godoy et al., 2009; Zettlemoyer et al., 2019). 75 Therefore, because phenological responses generate consistent shifts among species active at both ends of the flowering season, community-level changes in structural attributes of the 76 77 flowering season related to timing—such as its start, end, and duration—should be more strongly mediated by phenological responses than by range shifts (Fig. 1B-D) (Ramirez-Parada et al., 78 79 2025). Conversely, the richness of species flowering concurrently during a community's flowering peak—during which relatively few taxa are initiating or terminating flowering (Fig. 80 1B-D)—or attributes of the season tied to community composition (e.g., the network of 81 flowering synchronies between co-occurring species) (Fig. 1E, F) should be more strongly 82 83 influenced by species gains and losses due to range shifts than by plastic responses of flowering phenology. This is because phenological shifts redistribute existing flowering diversity and 84 change the degree of flowering synchrony between species (i.e., nodes in the flowering network), 85 86 whereas range shifts add or remove species from the community. Therefore, phenological shifts change the strength of the connections between nodes in the flowering network (Fig. 1E), 87 88 whereas range shifts add nodes or subtract them altogether, thereby creating or removing many connections at once (Fig. 1F). 89

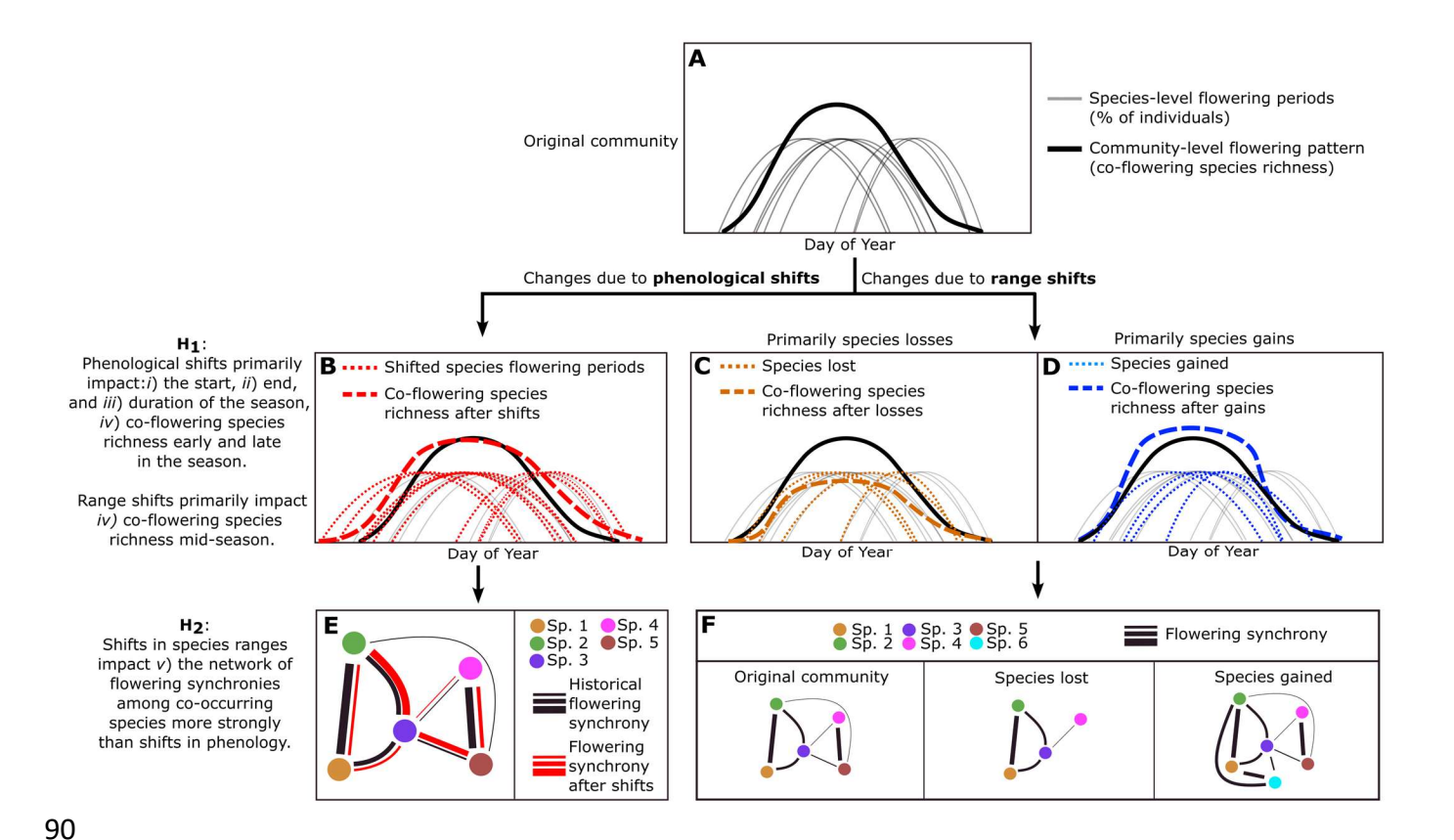


Figure 1—Hypothetical effects of shifts in phenology and species ranges on the structure of the flowering season at the community level. A shows historical phenological patterns in a community, with grey lines showing the flowering periods of individual species, and the solid black line depicting the historical species richness of coflowering species throughout the year. **B** shows changes in community-level flowering caused by shifts in phenology among species alone, and depicts a scenario in which early-flowering species tend to advance and lateflowering species to delay their flowering, and in which species primarily extend their flowering relative to historical. These changes are predicted to primarily impact the start, end, and duration of the season, as well as the richness of co-flowering species early and late in the season (H<sub>1</sub>). C and D show shifts in community-level flowering patterns caused by shifts in species ranges alone, respectively showing scenarios in which range shifts generate species losses or species gains in the focal community, and assuming gained or lost species do not tend to flower during a specific season. Such changes should primarily impact the richness of co-flowering species during the peak of the season, during which most species gained or lost are likely to have already started flowering (H<sub>1</sub>). E shows the effects of phenological shifts on patterns of pairwise flowering synchronies for a simple network of 5 species, and F depicts the effects of species losses or gains due to range shifts on the same network, with line widths indicating the degree of flowering synchrony between two species. Line colors in E depict flowering synchronies before and after shifts in flowering phenology due to environmental change. Shifts in phenology should alter the degree of overlap between species, with the weakest links most at risk of being lost under environmental change. In

91

92

93

94

95

96

97

98

99

100

101

102

103

104

105

106

turn, species losses or gains should have more profound effects by creating or removing flowering synchronies among many species at once (H<sub>2</sub>).

110

111

112

113

114

115

116

117

118

119

120

121

122

123

124

125

126

127

128

129

130

131

132

133

134

135

136

137

108

109

To test these hypotheses, we assembled a dataset of over 2.7 million herbarium and community-science records from 2,837 species, and examined how climate change affects the structure of the flowering season in the conterminous United States (CONUS). We modeled each species' geographic distribution under historical, current, and future climate conditions, also accounting for land cover and land use changes. Additionally, we assessed how temperature and precipitation—the main drivers of interannual variation in flowering time across the temperate zone—independently and interactively influence the onset and termination of the flowering period (and therefore its duration) for each species. By concurrently estimating species occurrences and their flowering periods across sites, these analyses allowed us to evaluate the effects of environmental change on flowering patterns at scales ranging from individual species to communities, and from local to continental extents. Specifically, throughout CONUS, we measured how recent and future environmental change affects community-level attributes of the season, including i) the start of the flowering season (SOS), ii) the end of the flowering season (EOS), *iii*) the duration of the flowering season (DOS), *iv*) the richness of co-flowering species each day of the year, and v) the network of pairwise flowering synchronies between co-occurring species, which determines the potential for flowering-mediated interactions between species. These metrics allowed us to evaluate the relative influence of shifts in phenology and species ranges on the timing of the season and the seasonal distribution of co-flowering richness within it (H<sub>1</sub> in Figs. 1B-D; attributes *i-iv* above) and in the network of flowering synchronies among cooccurring species (H<sub>2</sub> in Figs. 1E,F; attribute *v* above).

The impacts of shifts in phenology and species ranges are likely to differ across regional floras, as baseline climate, land use patterns, species assemblages, and rates of environmental change vary widely with geography. To characterize this regional variation, we evaluated how changes in each structural attribute of the flowering season (*i-v* above) varied throughout CONUS. Specifically, we evaluated patterns of change across ecoregions, which represent areas with relatively homogenous soils, geography, climates, and species assemblages (Omernik, 1987). In particular, we chose to summarize patterns within Level II ecoregions because they

provide a tractable number of subdivisions for analysis while maintaining resolution of regional subtypes within broad biomes (e.g., cold versus warm deserts, temperate versus semi-arid prairies, etc.). By doing so, these analyses offer the most comprehensive assessment of how recent and projected global change impacts flowering patterns across CONUS' floras, revealing wide heterogeneity in the severity of flowering reassembly among biomes.

143

144

145

146

147

148

149

150

151

152

153

154

155

156

157

158

159

160

161

162

163

164

165

166

138139

140

141

142

## **Materials and Methods**

Phenology and occurrence data

To model flowering phenology, we compiled specimen records from 220 herbaria, accessed digitally through 16 consortia from Mexico, the U.S., and Canada (in July and August 2022) (I. Park et al., 2023). Only specimens explicitly recorded as bearing flowers were retained, which we identified through the detection of unique entries in the DarwinCore 'reproductiveCondition' column that clearly indicated the presence of flowers. Specimens missing geographic coordinates, collection dates, or species-level identification were excluded. To avoid pseudoreplication, conspecific specimens collected within 1 km of each other on the same day were removed. Since over 92% of the remaining specimens were collected within the United States, and to match the spatial extent of land use/land cover (LULC) data used in species distribution models (SDMs), we excluded specimens collected outside CONUS. Specimens collected before 1958 were also removed to align with the temporal range of TerraClimate climate data used in the analysis. After harmonizing species names using the Global Biodiversity Information Facility (GBIF) taxonomic backbone, the data were filtered further to include only species represented by at least 100 specimens, a threshold past which the performance of specimen-based phenoclimatic models has been found to be independent of sample size (I. W. Park & Mazer, 2018). The day of year (DOY) of collection was used as a proxy for flowering date, with an azimuthal correction applied to address the discontinuity between 31 December and 1 January, converting prior year DOYs into negative values. Previous work on this dataset demonstrated limited spatial biases towards areas of high population density and major roads, and minor temporal biases that did not affect phenoclimatic model performance (Ramirez-Parada et al., 2024) (see Supplemental notes 7 and 8 therein).

To model species ranges, we obtained an additional 13.2 million research-grade occurrence records from GBIF for species well-represented in the flowering phenology dataset (accessed July 11, 2024; https://www.gbif.org/occurrence/download/0021084-240626123714530). These records, primarily from *iNaturalist* and herbarium sources, were combined with those from Park et al. (I. Park et al., 2023). We removed duplicates using the 'occurrenceID' column in DarwinCore. To match the temporal and spatial extent of LULC data included in SDMs, we retained only occurrences derived from iNaturalist and herbarium records collected between 1999 and 2023, and limited the dataset to occurrences within CONUS. Preliminary analyses of GBIF occurrences revealed significant spatial biases towards urban areas and major roads. To address this, we identified occurrences within urban areas as defined by the US Census Bureau (2012) using the 'tigris' package v2.1 (Walker, 2016). We thinned the data using the 'spThin' package v0.2.0 (Aiello-Lammens et al., 2015), keeping only occurrences of the same species recorded at least 20 km apart within urban areas. Additionally, we removed occurrences within 2 km of 'primary roads' mapped by the US Census Bureau in 2012. To further reduce spatial bias, another thinning step was applied, keeping only conspecifics recorded at least 5 km apart regardless of urban or road proximity. After cleaning using BONAP records (see next subsection), we retained only species with at least 50 occurrences to ensure adequate sample sizes for species distribution modeling (see 'Training SDMs' section for information on how pseudo-absences were generated). GBIF records were used in SDMs but not in phenology models because the vast majority of iNaturalist records do not indicate the presence of flowers.

187

188

189

190

191

192

193

194

195

196

167

168

169

170

171

172

173

174

175

176

177

178

179

180

181

182

183

184

185

186

## Final cleaning of specimens and occurrences using BONAP

Species misidentifications or geolocation errors in herbarium and occurrence databases can distort the climate space or flowering dates represented among observations. To mitigate this, we removed implausible records using expertly curated data from the Biota of North America Program's (BONAP) North American Plant Atlas (NAPA) (Kartesz, 2024), which documents 19,039 taxa from 227 families across 3,067 counties across CONUS. BONAP compiles species presence/absence data from herbarium records, museums, and bibliographic reviews, most of which are verified by taxonomic and floristic experts. We then excluded observations from counties where BONAP did not report occurrences for the species. After

cleaning, the final specimen-based phenology dataset included 1,042,939 specimens (collected from 1958 to 2022) representing 2,837 species in 1,042 genera and 139 families. The median species in the phenology dataset was represented by 242 specimens sampled in 54 unique years (median range = 62 years) by 122 unique collectors. The final occurrence dataset contained 1,673,454 records (collected from 1999 to 2023), comprising the same species. The median species in the occurrence dataset was represented by 347 observations sampled in 25 unique years (median range = 25 years) by 219 unique collectors. Among species in the data, 12% consisted of graminoids, 74% of herbs and forbs, 13% of woody species (shrubs or trees), and 1% of vines (Table S1).

## Climate data

We obtained monthly climatic rasters from TerraClimate (Abatzoglou et al., 2018) available from January 1958 to December of 2023 at a 4 × 4 km resolution. These data consisted of monthly time series for minimum temperature (TMIN), mean temperature (TMEAN), maximum temperature (TMAX), and cumulative precipitation (PPT), as well as modeled water balance metrics including actual evapotranspiration (AET), climate water deficit (DEF, potential evapotranspiration - AET), soil moisture (SOIL), and snow water equivalent (SWE).

## Climate variables for species distribution modelling

We used monthly climate data to calculate annual bioclimatic variables known to influence plant distributions. For each year and location across CONUS, we computed annual means (or sums for precipitation), minimum and maximum monthly values (e.g., mean minimum temperature of the coldest month, mean maximum of the warmest month), annual ranges (difference between maximum and minimum mean monthly values), and seasonality (standard deviation of monthly values within year). For temperature, we also calculated the approximate mean diurnal temperature range (mean difference between TMAX and TMIN across months) and approximate isothermality (mean approximate diurnal range divided by the annual range). For precipitation, seasonality was calculated relative to cumulative annual precipitation within each site. Minimum monthly SWE was removed from the analyses, as it was 0 across CONUS. This resulted in 31

climate variables: 7 for temperature, 5 related to PPT, AET, DEF, SOIL, and 4 for SWE, calculated annually across all CONUS locations. For the location of each occurrence record, we computed long-term averages of these variables over the 20 years preceding its collection date. We used 20-year instead of a standard 30-year period to reduce the proximity between historical and recent conditions in our analyses of species ranges (see next sections). Additionally, we obtained elevation data from USGS at a 100m × 100m resolution, and calculated mean elevation and elevational heterogeneity within 800m × 800m grid cells. The coarser resolution for elevation was used to account for uncertainties in georeferencing of herbarium specimens, which may be problematic in steep mountainous regions where topography changes over short distances (Gamble & Mazer, 2022).

Since many of the climate variables were highly collinear (Fig. S1) and are causally related, we performed a principal component analysis (PCA) to reduce the dimensionality of the climate space. The PCA used 20-year averages of all variables for the most recent period available (2004-2023) across all 4km  $\times$  4km grid cells in CONUS. We retained the five principal components (PCs) with eigenvalues  $\ge 1$ , which collectively explained 88.2% of the variance in the climate data (Table S2). PC1 represented a gradient of increasing aridity, PC2 a gradient of decreasing temperature and increasing temperature seasonality, and PC3 a gradient of increasing elevational heterogeneity and mean elevation with decreasing temperature seasonality. PC4 primarily captured increasing soil moisture, while PC5 reflected increasing actual evapotranspiration and elevation (Fig. S2). We then projected the 20-year average climate conditions associated with each occurrence record onto these PCA axes, reducing the number of climatic predictors from 31 variables to 5.

To predict species distributions across different periods, for each occurrence record we calculated 20-year averages for each of the 31 climate variables for a historical period (1961-1980; representing the earliest 20-year period available in TerraClimate) and a recent period (2001-2020; to ensure separation with the historical period). We also obtained projected climate conditions from TerraClimate for a scenario where global temperatures rise by 2°C above preindustrial levels. This scenario is not tied to a specific time frame or emissions pathway; instead, TerraClimate interpolates climate normals from 1985-2015, adjusting for the changes in means

and seasonality expected under 2°C of warming. We then projected historical, recent, and future climatic conditions onto the 5 principal components derived from the 2001-2020 data.

257

258

259

260

261

262

263

264

265

266

267

268

269

270

271

272

273274

275

276

277

278

279

280

281

255

256

## Climate variables for phenoclimatic modelling

Variation in TMEAN and PPT among sites and years of specimen collection was partitioned into spatial and temporal components by calculating long-term means (reflecting geographic differences in chronic climatic conditions) and year-specific deviations from these long-term means (reflecting interannual differences). For each species at each site and year, we obtained data for the climatic conditions during the 3-month periods leading up to its average flowering onset, peak, and termination. To estimate conditions approximately before flowering onset, we used the 10th percentile collection date across all specimens from each species and calculated the mean TMEAN and cumulative PPT for the 3 months leading up to that month. The same approach was applied for the 50th percentile (flowering median) and 90th percentile (flowering termination) collection dates. These percentiles were chosen to prevent sample-size dependent biases likely to occur for more extreme quantiles, and because they have been found to perform well in specimen-based quantile regressions of phenology (I. W. Park et al., 2024). For each specimen, we characterized its site's long-term TMEAN and PPT (normals) by averaging the observed conditions across all years between 1961 and 1990 for each 3-month period approximating that species' flowering onset, median, and termination. We then calculated climatic deviations (anomalies) from the 1961-1990 normals in the year of each specimen's collection for these 3-month periods.

As phenological changes are driven by interannual variation in TMEAN and PPT (and through plastic responses) (Ramirez-Parada et al. 2024), we calculated deviations from 1961-1990 normals for all 3-month windows. This was done for the historical period (1961-1980), the recent period (2001-2020), and the future 2°C warming scenario. These TMEAN and PPT deviations were then used to predict changes in flowering onset and termination between reference periods at each species' occurrence site.

282

283

## Land use and land cover data

We obtained land use and land cover (LULC) data from the National Land Cover Database (NLCD) (Jon Dewitz, 2024), available for 2001, 2004, 2006, 2008, 2011, 2013, 2016, 2019, and 2021. The NLCD uses Landsat spectral data to classify 30m resolution grid cells into land cover and land use classes, providing a consistent, high-resolution dataset across CONUS. We separated each year's multiclass raster into layers representing the presence or absence of each LULC type. We retained all cover classes except those not found in CONUS (e.g., lichen, moss, sedge classes from Alaska) or those that were rare (e.g., barren land). For land cover, we kept forest classes (deciduous, evergreen, mixed), scrubland (shrub/scrub), herbaceous grasslands, and wetlands (herbaceous and woody). For land use, we included four urban categories (open, low, mid, high) and two agricultural classes (cultivated crops, pasture/hay). To match the format of the LULC data available for forecasting and backcasting (see next paragraph), we aggregated all urban classes into a single category. To account for uncertainty in occurrence coordinates and because plant occurrence can be influenced by landscape context at broader scales than 30m (Mazerolle and Villard, 1999), we measured the proportion of each class cover within 750m × 750m grid cells (625 30m × 30m cells) around each occurrence. LULC class proportions were sourced from the NLCD layer closest to the year of collection for each record. These class proportions were then used as predictors in SDMs.

Because NLCD data were available only from 2001 to 2021, we obtained historical (1961-1980) and future (2061-2080) LULC projections from the Earth Resources Observation and Science Center (EROS) at a 250m resolution (T. Sohl et al., 2016; T. L. Sohl et al., 2014). EROS' projections use the same modeling framework as NLCD, integrating land use trends with spatially explicit allocation based on regional suitability for each LULC class. Though EROS projections were based on the Special Reports Emissions Scenarios (SRES) from the IPCC (2000)—replaced later by Representative Concentration Pathways (RCP; IPCC 2013) and Shared Socioeconomic Pathways (SSP; IPCC 2021)—they align closely with RCP and SSP scenarios (Riahi et al., 2017; Rogelj et al., 2012). We chose the B1 scenario for forecasting, as it is the closest match to RCP4.5 and SSP2-3, representing 'middle-of-the-road' emissions and development scenarios. As with NLCD data, we calculated the proportion of each land cover class in 750m resolution blocks (containing 9 grid cells) to generate historical and future predictions used in SDMs.

Analyses

## Training SDMs

Species distributions were modeled using presence-background random forest classifier models implemented in the 'randomForest' package v4.7-1.1 (Liaw & Wiener, 2002) in R. Random forests are a supervised machine learning technique that uses an ensemble of decision trees to identify relationships between a response (here, presence/background data) and predictors (here, climatic and LULC variables). By combining multiple decision trees, the ensemble performs better than any single model, leveraging the "wisdom of the crowds." This approach does not require predefining model structures (e.g., linear relationships) and its non-parametric nature allows for discovering complex relationships and interactions (Cutler et al., 2007). This flexibility was crucial for analyzing thousands of species presumably representing diverse distributional relationships with climate and LULC. Additionally, random forests are computationally efficient and have been demonstrated to be among the most accurate SDM methods available (Valavi et al., 2022).

SDMs for each species were trained using occurrence data from 1999-2023. This period ensured availability of high-quality LULC data from NLCD within two years of each collection date. We generated pseudo-absences for each species by sampling 10,000 random locations per species using three alternative types of geographic stratification, fitting a separate SDM for each one and selecting the approach yielding the highest performance on a validation set for the rest of the analysis pipeline. The first approach followed methods by Barbet-Massin et al. (Barbet-Massin et al., 2012) in which, for each species, we defined a large region around the occurrences of each species that excluded areas within a 1° radius around each observation. Specifically, we defined the sampling area for each species using a 2° buffer (~222 km) around the convex hull encompassing all occurrences. To tailor this approach to species with discontinuous distributions, our second approach defined the pseudo-absence sampling area using a 2° buffer around the minimum density kernel estimated to encompass all occurrences of the species. This way, the sampling regions could be discontinuous, avoiding sampling pseudo-absence disproportionately from areas far from any occurrences. To account for differences in range size, this approach tailored the radius of the exclusion buffer around each occurrence to a 20<sup>th</sup> of the

minimum between the latitudinal versus longitudinal among the species' occurrences. Finally, because its typically unclear whether regions without occurrences are due to sampling bias or true distributional patterns, our third approach used curated BONAP records to identify counties where each species has not been documented to date. This approach increases the likelihood that pseudo-absences indeed represent true absences at the risk of losing resolution of the environmental space in regions where the species does occur. For each approach, pseudo-absence sampling also excluded locations within 2km of major roads.

344

345

346

347

348

349

350

351

352

353

354

355

356

357

358

359

360

361

362

363

364

365

366

367

368

369

370

371

372

373

All models included the 5 bioclimatic PCs and the proportion of each LULC class around collection sites as predictors. In the case of pseudo-absences, we obtained 20-year climatic averages from a randomly selected year between 2001 and 2021 projected onto the 5 climatic PCs and LULC variables. To address class imbalance, we downsampled pseudo-absences to match the number of occurrences in each initial tree. Each species-specific model used 500 trees with a maximum of 5 predictors at each split. Decision trees are built using bootstrap samples of the data. Typically, these samples contain about 2/3 of the original data, with the remaining third (out-of-bag or 'OOB' data) used to calculate each tree's error rate (Cutler et al. 2007). We evaluated model performance by averaging the error rates across all trees, which typically provides an unbiased estimate of the model's generalization error. Specifically, we calculated the area under the receiver operating characteristic curve (AUC) using OOB samples, which quantifies the tradeoff between false positive and false negative rates for different threshold values used for classifying presences versus absences. Fully random models would yield an expected AUC of 0.5, with values below that indicating worse-than-random performance, and higher values better-than-random performance. We identified the pseudo-absence approach yielding the best performing model by comparing the AUCs for each species' SDM. The first approach was best performing only among 8% of species, whereas the second and third approaches were best performing among 29% and 63% of species, respectively. After model selection, the median AUC among species was 0.996 (min = 0.90).

The SDMs output a probability of occurrence under specific environmental conditions, derived from the proportion of trees predicting the positive class. Given that SDMs were fit with observed presences but generated pseudo-absences data, these probabilities are interpreted as habitat suitability rather than actual probabilities of occurrence. To set a suitability threshold (0-

1) for considering a species to be present at a site, we calculated the receiving operating curve (ROC) for each model and determined which of two criteria yielded the best predictive power: 1) maximizing the sum of specificity and sensitivity, or 2) maximizing the true positive rate (minimizing false negatives) while keeping the false positive rate below 0.05. While the first criterion maximized the true skill of the model, the second criterion maximized true positive detection at the expense of higher false negative rates, a tradeoff that is justified in our case since implausible occurrence predictions could be identified and removed using BONAP county records (see 'Species-level predictions of distributions and phenology' subsection).

## Training phenoclimatic models

For each species, we modeled how flowering onset, termination, and duration varied with long-term climatic conditions and interannual climatic variation. We used quantile regression (via the 'quantreg' package v5.97) (Koenker et al., 2017) to assess how collection date distributions among conspecifics responded to geographic and interannual variations in TMEAN and PPT (i.e., normal and anomalies, respectively). We used the 10th percentile of the distribution to represent population-level flowering onset, the 90th percentile to represent flowering termination, and the interquartile distance between them to represent flowering duration. We chose the 10th and 90th percentiles and focused on well-sampled species because estimation of extreme quantiles is more strongly biased by small samples. Moreover, recent simulations show that quantile regression accurately estimates 10<sup>th</sup> and 90<sup>th</sup> percentiles of opportunistically sampled data for sample sizes similar to those in this study (I. W. Park et al., 2024), and this approach has been effective in studying phenological distributions in both plants and insects (Austin et al., 2024; Belitz et al., 2023).

In each species-specific model, predictors included TMEAN normal, PPT normal, and their interaction for the 3-month period before the approximate date of flowering onset (10<sup>th</sup> percentile DOY among specimens) or termination (90<sup>th</sup> percentile DOY), as well as TMEAN anomaly, PPT anomaly, and their interaction during the same period (6 predictors total). The coefficients for the main terms in these quantile regressions indicate how the 10th and 90th percentiles of flowering are affected by geographic or interannual variation in TMEAN and PPT, assuming average values for interacting variables. Interaction coefficients between normals

represent the degree to which long-term precipitation affects the magnitude of phenological changes due to variation in long-term TMEAN across sites (or vice versa), whereas the interaction coefficients between anomalies indicate how the effects of interannual variation in TMEAN varies among drier- or wetter-than-average years (and vice versa). This approach models phenological variation as a response to: i) geographic variation in chronic TMEAN and PPT conditions across sites, using temporally invariant normals from 1961-1990, and ii) TMEAN and PPT anomalies reflecting temporal variation within sites, which primarily capture plastic phenological responses (Ramirez-Parada et al., 2024). Thus, we assumed that any temporal changes in a species' flowering season within sites are driven by deviations from their 1961-1990 TMEAN and PPT normals.

# Species-level predictions of distributions and phenology

Each species' SDM was used to generate habitat suitability maps for historical (1961-1980), recent (2001-2020), and future (2 °C warming, B1 LULC scenario for 2080) conditions. Climatic and LULC variables were resampled to a 12km resolution for computational ease. Suitability estimates were then converted to binary occurrence maps by applying a threshold that maximized the true positive rate (see 'Analyses—Training SDMs' subsection). Presence-only SDMs can predict unsuitable areas outside a species' range or beyond its dispersal capacity. To address this, predictions were constrained to within 40km of counties where BONAP confirmed each species' presence, which allowed for moderate range expansion to areas adjacent to currently occupied regions between periods. These SDMs predicted substantial variation in species richness across CONUS, from 56 to 1,445 species (from a total 2,837) for the historical period (Fig. S3). Species richness was generally lowest in arid regions of the Great Plains and higher in the West compared to the East, consistent with more comprehensive assessments of plant diversity in North America (Daru, 2024). The proportion of species of different growth forms represented within communities varied moderately across CONUS (Fig. S3), and growth forms did not differ substantially in their average degree of range change between periods (Fig. S4).

Each species' phenoclimatic model was used to predict flowering onset, termination, and duration for each 12km×12km grid cell where the species was projected to occur during

historical, recent, and future periods. This was done by applying deviations of average TMEAN and PPT conditions from the 1961-1990 normals for each period. Climate rasters were resampled to a 12km resolution before estimating phenological onset, termination, and duration for each site and period. Species in different growth forms did not exhibit substantially different degrees of onset and termination sensitivity to temperature and precipitation (Fig. S5).

## Changes in community composition and flowering structure

The SDM and phenoclimatic modeling provided predictions for species presence, flowering onset, and termination under historical, recent, and future conditions. We used these predictions to measure changes in species composition. Next, we examined changes in the start, end, and duration of the flowering season across these periods. The start of the flowering season was defined as the DOY when 5% of species had started flowering, and the end as the DOY when 95% of species had ceased flowering, with duration as the span between these dates. For each location, we calculated the difference in days for the season's start, end, and duration between historical and recent conditions, and between recent and future conditions. We also measured changes in the richness of flowering species each month by calculating the proportional difference in species numbers under historical versus recent and recent versus future conditions, relative to local species richness in the preceding period.

Finally, we assessed how patterns of flowering synchrony among species change in response to environmental trends. For each location, we first calculated the overlap in flowering periods between each pair of species in each period, calculating changes in overlap between historical and recent conditions, or recent and future conditions. Specifically, synchrony was calculated as:

# Overlap between A and B Flowering period of A + Flowering period of B - Overlap between A and B

Therefore, pairwise synchrony ranged from 0 (no overlap) to 1 (identical and fully overlapping flowering dates). For species present in one period but not the other, all flowering synchronies were set to 0 for the period in which it was absent. Using these pairwise overlaps, we measured changes in flowering synchrony within each community using the Bray-Curtis Dissimilarity

Index (BCI) (Bray & Curtis, 1957). While BCI is typically used to assess species composition dissimilarity between communities using abundance data, it is also applicable to other categorical data. In this context, BCI measured compositional differences in flowering overlaps between periods, with species pairs analogous to species and their degree of flowering synchrony analogous to abundance. Therefore, the BCI provides an integrated measure of changes in both the identity and degree of overlap among species pairs, with values ranging from 0 (complete similarity) to 1 (complete dissimilarity) between periods for each community.

469

470

471

472

473

474

475

476

477

478

479

480

481

482

483

484

485

486

487

488

489

490

462

463

464

465

466

467

468

Phenology versus range shifts as drivers of community-level phenological change

To assess the relative contributions of shifts in phenology and species ranges to the resulting shifts in structure of the flowering season in each location, we generated predictions of community level change assuming that either i) phenology changed but species distributions remained constant between periods (i.e., a 'phenology-only' scenario), or ii) phenology remained constant but distributions changed between periods (i.e., a 'distributions-only' scenario). For example, for scenarios in which only phenology shifted between historical and recent periods (i.e., 1961-1980 to 2001-2020), we generated species ranges predicted using historical climate and LULC conditions, and compared flowering dates predicted under historical versus recent conditions within these historical ranges. For each attribute of the season—and for all comparisons between historical, recent, and projected environmental conditions—we then calculated the difference between estimates of change generated by shifts in both species ranges and phenology (shown in the main text) and those obtained by allowing only phenology or distributions to shift. Changes in community-level attributes of the season at a location were classified as predominantly driven by phenological shifts if closest to the change observed in the phenology-only scenario, or classified as predominantly driven by range shifts if closest to the distributions-only scenario. Finally, to assess the predominance of phenological versus range shifts as drivers of change across biomes, we calculated the proportion of grid cells in each Level II ecoregion within CONUS for which each process was the predominant driver of observed changes. When doing this for changes in the richness of flowering species each month, we excluded locations showing shifts of less than 0.01 (corresponding to 1% of local species

richness) each month, as those overwhelmingly corresponded to areas where the flowering season had not yet started or had already ended.

493

491

492

494

495

496

497

498

499

500

501

502

503

504

505

506

507

508

509

510

511

512

513

## Results

Changes to the start, duration, and end of the flowering season

Estimated shifts in species ranges and flowering phenology generated consistent changes to the flowering season's start (SOS), end (EOS), and duration (DOS) across most ecoregions. SOS predominantly advanced between the historical and recent periods (Fig. 2A). EOS was delayed in Eastern ecoregions, while responses in the West were more variable (Fig. 2A). Nonetheless, SOS and EOS generally moved in opposite directions, with SOS showing larger shifts towards earlier dates where SOS and EOS moved in the same direction; consequently, the flowering season duration (DOS) increased across most of CONUS (Fig. 2A). Future environmental conditions were projected to generate more drastic changes, with greater SOS advances and more consistent EOS delays than in recent decades (Fig. 2B). As a result, DOS was predicted to increase further across most of CONUS (Fig. 2B). Across ecoregions, shifts in the timing of the season between the historical and recent periods were primarily caused by shifts in flowering phenology (Fig. 2C). However, in most ecoregion, seasonal changes within a substantial proportion of sites were caused primarily by estimated shifts in species ranges, which predominated overall as drivers of EOS shifts in some ecoregions (e.g., Upper Gila Mountains) (Fig. 2C). Phenological shifts were also projected to be the primary drivers of changes in SOS, EOS, and DOS between recent and future climatic conditions in most ecoregions (Fig. 2C).

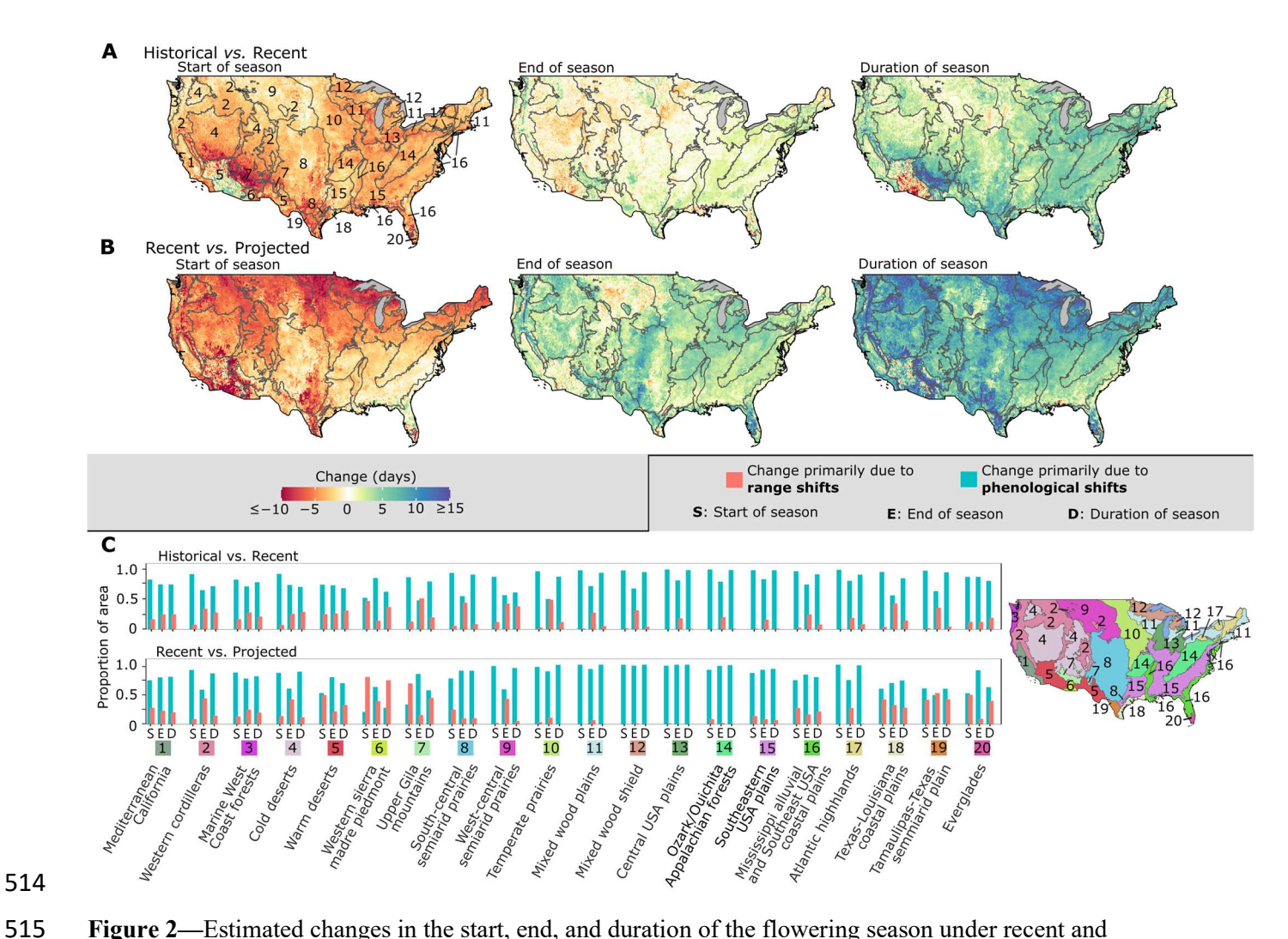


**Figure 2**—Estimated changes in the start, end, and duration of the flowering season under recent and projected climatic and land cover change, and the relative contributions of shifts in phenology vs. species ranges to these changes. **A** depicts changes in the start, end, and duration of the season predicted between the historical (1961-1980) and recent (2001-2020) periods. **B** shows predicted changes between recent conditions and future conditions expected under 2°C of warming and land cover patterns for the year 2080 under the Special Report on Emissions Scenario (SRES) B1. **C** shows the proportion of area within each level II ecoregion throughout CONUS (map subdivisions labeled 1-20, also shown in A) for which shifts in phenology or in species ranges were the primary contributors to observed change. For graphing, the color scale in **A** and **B** was capped to the central 99% of the data to avoid distortion of the range from extreme values. Grid cells in **A** and **B** have a resolution of 12×12 km.

Changes in the seasonal distribution of co-flowering species richness

Co-flowering species richness was estimated to remain mostly unchanged during the winter months preceding the flowering season, but to increase by February in low-latitude ecoregions where spring starts early (e.g., Warm Deserts) (Fig. 3A). Significant changes were widespread in

March, April, and May, which predominantly showed increases due to the earlier onset of spring across CONUS. Decreases first occurred in April and May in regions experiencing early onset of summer drought (e.g., Warm Deserts, South-Central Semi-Arid Prairies). More ecoregions experienced declines in co-flowering richness during summer, with the onset of declines occurring earlier in the year in arid ecoregions (e.g., May to June for Cold Deserts vs. June to July for the Western Cordillera). Fall changes were modest across CONUS. In all ecoregions, changes in co-flowering species richness early in the season were primarily generated by phenological shifts, with range shifts exerting a greater influence later in the season and predominating during late spring and summer (May-Sep; Fig. 3B). The predominant drivers of changes in co-flowering species richness near the end of the season varied among ecoregions, with shifts in phenology predominating in some (e.g., Warm Deserts) and range shifts in others (e.g., Temperate prairies).

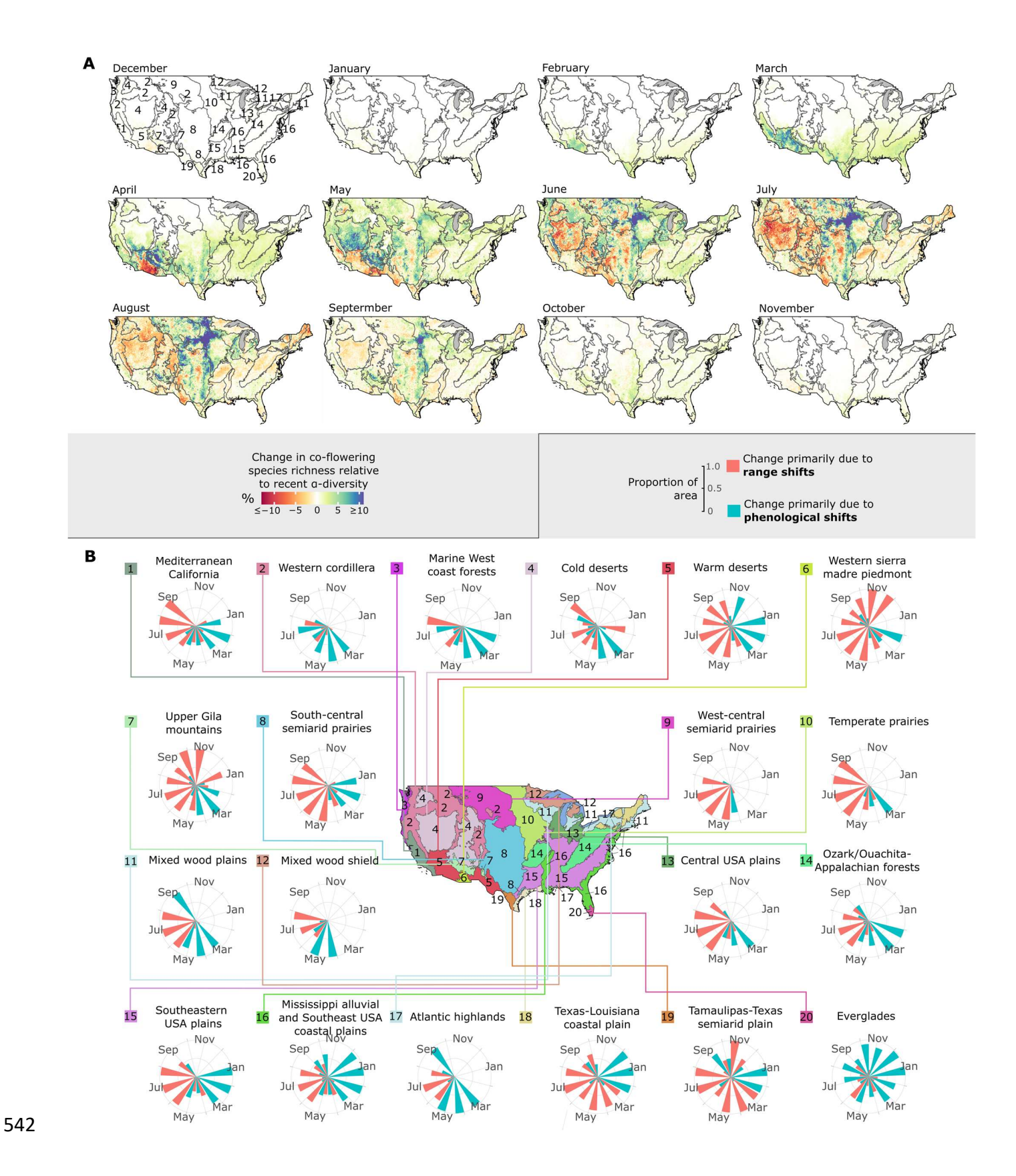


**Figure 3**—Estimated changes between the historical period (1961-1980) and the recent period (2001-2020) in the richness of co-occurring species flowering each month across the conterminous United States. **A** shows the change co-flowering richness each month for each location relative to the total species diversity of that site during the historical period (1961-1990). **B** shows the proportion of sites within each ecoregion (map subdivisions labeled 1-20) for which range shifts or phenological shifts were the primary cause of observed changes in the diversity of flowering species that month. For graphing, the color scale in **A** was capped to the central 99% of values to avoid distortion from extreme values. Grid cells in **A** have a resolution of 12×12 km.

551

552

553

554

555

556

557

558

559

560

561

562

563564

565

566

567

543

544

545546

547

548

549

550

Under projected climate conditions, estimated decreases in co-flowering species richness were greater and more widespread across ecoregions than in recent decades (Fig. 4). Increases during spring were weaker, and declines occurred earlier and were more severe in many ecoregions (e.g., Warm Deserts, Mediterranean California) (Fig. 4A). Summer and fall decreases were most severe across ecoregions in the Great Plains, but were also widespread across the West. In contrast, co-flowering species richness was projected to moderately increase during summer and fall in many Eastern ecoregions (e.g., Southeast USA Plains, Southeast USA Coastal Plain). For most ecoregions, phenological shifts are projected to be the primary causes of changes in co-flowering species richness early and late in the season (Fig. 4B). Phenological shifts predominated throughout most of the year in some ecoregions (e.g., Mixed Wood Shield, Mixed Wood Plains). However, the relative influence of range shifts increased throughout the year, becoming the predominant cause of year-round changes in co-flowering richness in more ecoregions than observed between the historical and recent periods (e.g., Texas-Louisiana Coastal Plain). Indeed, range shifts were the overwhelming cause of changes in co-flowering richness during summer and fall in regions showing the most severe decreases (e.g., South Central Semi-Arid Prairies, Temperate Prairies).

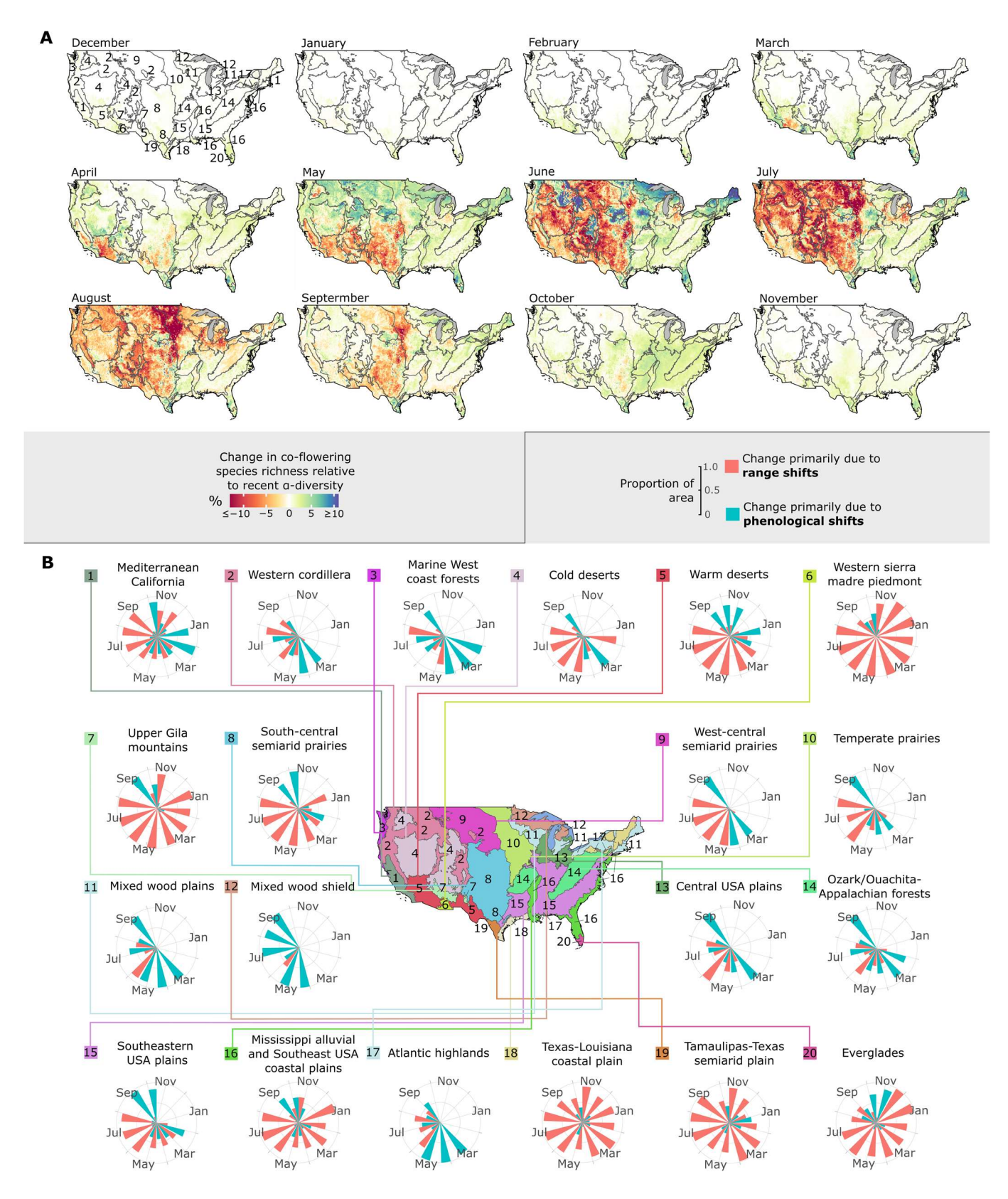


**Figure 4**—Estimated changes between recent and future environmental conditions in the richness of species flowering each month across the conterminous United States. The color scale in each panel shows

the projected change in co-flowering species richness each month in each location relative to the total species richness of that site estimated under recent environmental conditions (2001-2020). Projected conditions correspond to those expected under 2 °C of warming and land cover patterns for the year 2080 under the Special Report on Emissions Scenario (SRES) B1. A shows the change co-flowering richness each month for each location relative to the total species diversity of that site during the recent period (2001-2020). B shows the proportion of sites within each ecoregion (map subdivisions labeled 1-20) for which range shifts or phenological shifts were the primary cause of observed changes in the diversity of flowering species that month. For graphing, the color scale was capped to the central 99% of the data to avoid distortion of the range from extreme values. Subdivisions in each panel—labeled 1-20—represent level II ecoregions. Grid cells in A have a resolution of 12×12 km.

# Changes in patterns of pairwise flowering synchronies

Across periods, estimated changes in the composition of pairwise flowering synchronies among species in a community (i.e., flowering dissimilarity) largely corresponded with those in coflowering species richness during the peak of the season, with the greatest changes concentrated in ecoregions within central CONUS and in the West (Fig. 5A). Flowering dissimilarity between periods was more severe under projected environmental conditions than observed in recent decades, with the greatest dissimilarity observed across central CONUS and the West, and relatively modest flowering dissimilarity throughout the East (Fig. 5B). Flowering dissimilarity across periods was predominantly driven by range shifts among ecoregions (Fig. 5C). Indeed, in ecoregions showing the most severe flowering dissimilarity between periods, change across nearly all locations was primarily caused by range shifts (e.g., South-Central Semi-Arid Prairies).

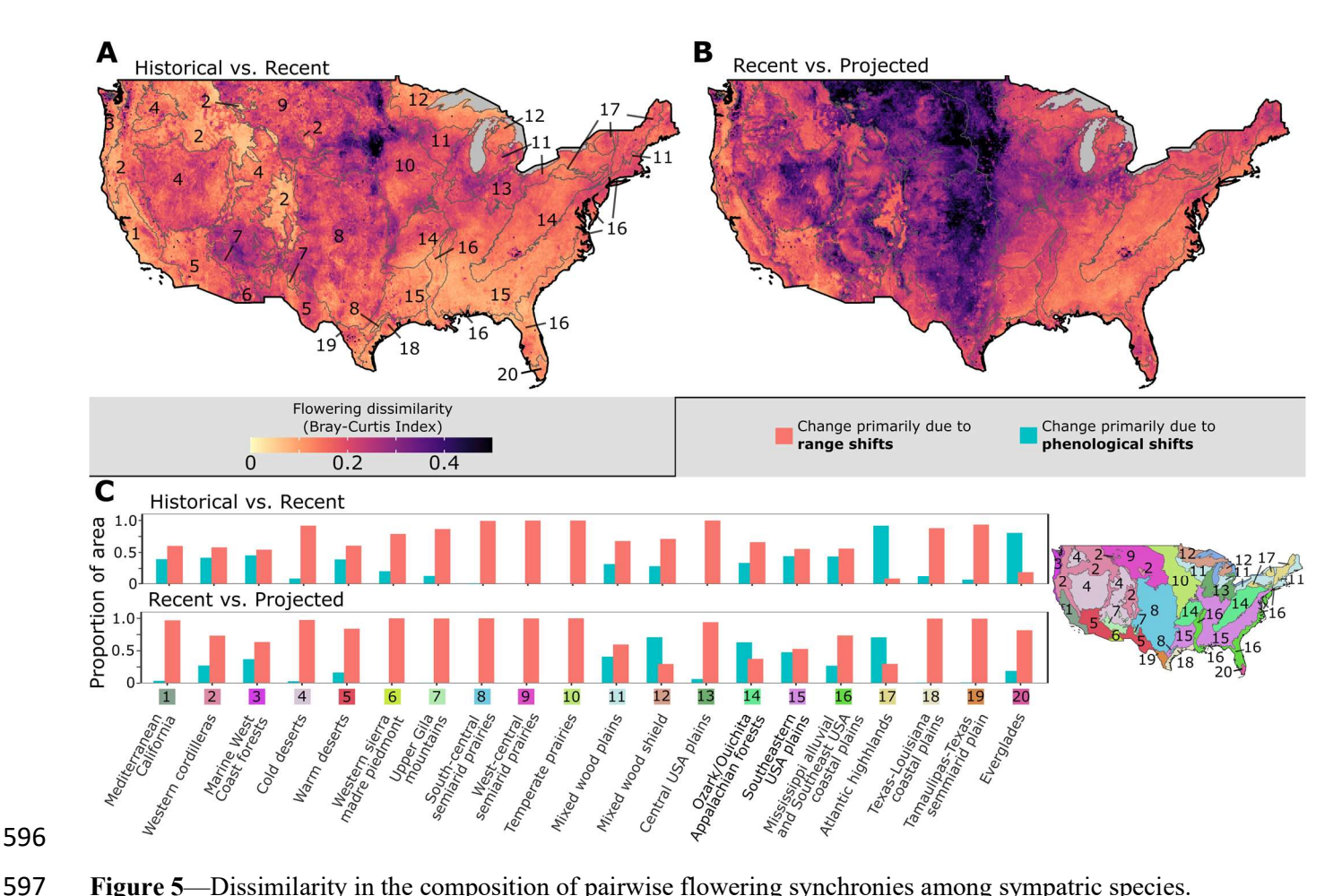


**Figure 5**—Dissimilarity in the composition of pairwise flowering synchronies among sympatric species. A shows flowering dissimilarity between the historical (1961-1980) and recent (2001-2020) periods. **B** shows flowering dissimilarity between recent and projected conditions, which correspond to those expected under 2 °C of warming and land cover patterns for the year 2080 under the Special Report on Emissions Scenario (SRES) B1. Flowering dissimilarity was measured using the Bray-Curtis Dissimilarity index, with values of 0 indicating no changes in species composition and degree of flowering overlap, and values of 1 indicating all pairs of overlapping species were gained or lost relative to the preceding period. For graphing, the color scale was capped to the central 99% of the data to avoid distortion of the range from extreme values. Subdivisions in each panel—labeled 1-20—represent level II ecoregions. **C** shows the proportion of area within each ecoregion in which either shifts in phenology or species ranges was the primary cause of flowering dissimilarity between periods.

## **Discussion**

By analyzing thousands of plant species, we demonstrate that joint shifts in phenology and species ranges in recent decades have significantly advanced and extended the flowering season across biomes in the United States. We found substantial seasonal redistribution of flowering

diversity within communities, with co-flowering species richness typically increasing early and late in the season and decreasing during historical peaks—trends predicted to intensify under projected environmental conditions. Despite acting concurrently, shifts in phenology versus species-ranges primarily impacted different attributes of the season. Species-level phenological shifts were the primary drivers of changes in community-level attributes related to the timing of the flowering season, such as its start, end, and duration. In contrast, changes in species' ranges were the main drivers of community-level shifts in co-flowering richness during late spring and summer and of attributes tied to community composition, such as patterns of flowering synchrony among co-occurring species. These findings outline heterogeneous macroecological impacts and mechanisms of change across biomes, revealing a wider suite of impacts than predicted from analysis of each process in isolation.

Shifts in phenology and species distribution jointly but distinctly impact the flowering season. As hypothesized (Fig. 1), shifts in phenology and range shifts had their greatest effects on different attributes of the flowering season at the community level. This suggests that future changes to the structure of the season across communities will depend on the relative severity of concordant shifts in phenology versus species ranges. Specifically, predominance of phenological shifts would primarily alter the timing of the flowering season and the seasonal distribution and diversity of co-flowering species, particularly at the start and end of the season. In turn, profound species turnover due to range shifts would primarily alter seasonal peaks in flowering diversity and the network of flowering synchronies among species, thereby altering the potential for flowering-mediated species interactions.

The predominance of either process will likely depend on the severity of environmental trends. Limits to phenological plasticity can prevent plants from shifting development further in response to climatic trends (Rutishauser et al., 2008). For example, studies on woody species in the temperate zone have found that phenology shifts linearly with temperature up to a warming threshold of approximately 4 °C, after which responses stall (Ettinger, 2020; Fu et al., 2015; Guo et al., 2023). Therefore, while average global temperature changes of 2 °C—as those considered here—might not cause widespread exhaustion of plant phenological plasticity, these constraints might be important under more extreme warming scenarios, limiting further contributions of

shifts in phenology to changes in the flowering season. In contrast, shifts in demography and species ranges are likely to accelerate under more extreme environmental change (Feeley & Silman, 2010; Huntley, 1991). Therefore—to the extent that the limits of phenological plasticity are similar across biomes, functional groups, and taxa—more severe climate change could cause comparatively harsher shifts in species ranges than phenology, thus primarily impacting the diversity and synchrony of co-flowering species.

Flowering reassembly and its impacts differ across biomes

Our study corroborates previous research showing widespread advancement and lengthening of the flowering season across floras (Chen et al., 2023; Li et al., 2021; Zhou et al., 2022). However, we also found wide regional variation in the direction and severity of changes in the structure of the flowering season, which may cause profound ecological impacts. For example, in recent decades, the richness of co-flowering species sharply increased early and decreased later in the season in many ecoregions (e.g., Western Cordillera, Cold Deserts, Mediterranean California; Fig. 3), which could result in opposing effects on density-dependent processes such as pollinator attraction or insect foraging success during spring and summer (Schenk et al., 2018; Sponsler et al., 2023). In turn, some communities experienced consistent declines in flowering diversity throughout the year (e.g., areas of the South-Central Semi-Arid Prairies), which could decrease the diversity of organisms reliant on flowers across the season (Fründ et al., 2010; Potts et al., 2003). Other regions experienced consistent increases in flowering diversity throughout the year (e.g., Southeastern ecoregions), which may not affect different seasons disproportionately but could alter ecological processes through novel species interactions (Renner & Zohner, 2018). Regardless of specific patterns, these shifts have likely altered (and may continue to alter) the selective environments encountered by plants and interacting organisms across CONUS (Elzinga et al., 2007).

Communities across the Great Plains appear particularly vulnerable to climate-driven restructuring of the flowering season (Fig. 5). In recent decades, this region has experienced increasing aridity to the West and increasing humidity to the East of the 100th meridian West—a bioclimatic boundary dividing the humid East and arid West (Seager et al., 2018). Aridification has been linked to biomass loss, rapid species declines, and species turnover in grasslands (Chase

et al., 2000; Cleland et al., 2013; MacDougall et al., 2024). Climate change is predicted to exacerbate aridification trends, and conversion of grasslands to agriculture is projected to accelerate under the land use scenario considered in this study (Figs. S2,6), threatening pollinator diversity and associated ecosystem services (Woodcock et al., 2019). In contrast, many regions exhibit lower flowering reassembly despite facing aridification or substantial land cover changes (e.g., most Southeastern ecoregions) (Figs. S2,6). While we cannot identify the ultimate causes of these trends, the severe impacts expected across the Great Plains might be caused by potential limits to species ranges imposed by the arid-humid bioclimatic boundary, with aridification trends leading to local extirpation of humidity-adapted species at the boundaries of their ranges (Anderegg & HilleRisLambers, 2016; Barnes & Harrison, 1982; Berdugo et al., 2020; Epstein et al., 1996).

## Limitations and future directions

This study provides a unique macroecological assessment of changes to the flowering season due to the combined effects of shifts in flowering time and species ranges across the continental United States. However, methodological limitations and ecological complexities make the precise ecological consequences of these effects difficult to predict.. First, we modeled shifts in the timing and diversity of flowering across scales, but not in the overall abundance of floral resources due to potential changes in species' abundances or flower production, which could amplify or reduce the ecological impacts of altered flowering times. Relatedly, presencebackground SDMs model shifts in habitat suitability without accounting for temporal lags in colonization or local extinction, or the persistence of populations in suboptimal habitat potentially overestimating species turnover at short time scales—and do not consider changes in population sizes. Longitudinal field surveys are ultimately needed to determine whether estimated trends from SDMs match true patterns across landscapes. Finally, many plant communities are dominated by a few species whose flowering responses may deviate from the wider community, and ecological outcomes often depend on a handful of species interactions (e.g., specialized plant-pollinators systems) whose responses might not match those of the wider community.

Given these and other complexities, assessing the effects of climate change on floral resource production—both through individual-level crop sizes and population-level demography—is crucial to determine whether the spatiotemporal redistribution of co-flowering diversity will lead to concordant changes in floral resource availability. In turn, forecasting more precise ecological outcomes will require focusing analyses on key species based on local abundance, floral output, functional traits, or other attributes relevant to the specific ecological phenomena under study.

Despite these challenges, this study provides a promising approach for examining changes to the seasonal structure of terrestrial communities at broad spatial scales. Field datasets tracking the seasonal abundance of flowers are rare, and remote sensing methods cannot detect weak spectral signals from these structures nor identify individual species. By combining species distribution and phenological modeling and using diverse publicly available datasets, we outline a framework for estimating changes to the seasonal structure of plant communities at broad spatial scales that maintains resolution at the level of species, features that may provide valuable resources for natural resource management and conservation planning.

# Acknowledgements

- 720 This work was supported by the National Science Foundation through NSF DEB-1556768
- 721 (S.J.M. and I.W.P.), NSF DEB-2105932 (S.J.M. and I.W.P.), NSF DEB-2105907 (S.R.) and
- NSF DEB-2105903 (C.C.D.). T.H.R.-P. is grateful to the University of California, Santa
- 723 Barbara, for fellowship support in the year this manuscript was completed. We thank the many
- herbaria, including botanists, staff and volunteers, who collected, curated and digitized the vast
- volumes of herbarium specimens and community-science records leveraged for this study. We
- thank Elsa Cleland and Leander Anderegg for their insightful feedback on earlier versions of this
- 727 manuscript.

## Data and code availability statement

The underlying data used in the analyses—as well as all resulting estimates of species ranges and

- 731 spatially explicit phenological predictions—are publicly available on Zenodo
- 732 (https://doi.org/10.5281/zenodo.17429436).

## References

733

734 Abatzoglou, J. T., Dobrowski, S. Z., Parks, S. A., & Hegewisch, K. C. (2018). TerraClimate, a 735 high-resolution global dataset of monthly climate and climatic water balance from 1958– 736 2015. Scientific Data, 5(1), 170191. https://doi.org/10.1038/sdata.2017.191 737 Aiello-Lammens, M. E., Boria, R. A., Radosavljevic, A., Vilela, B., & Anderson, R. P. (2015). 738 spThin: An R package for spatial thinning of species occurrence records for use in 739 ecological niche models. Ecography, 38(5), 541–545. https://doi.org/10.1111/ecog.01132 740 Anderegg, L. D. L., & HilleRisLambers, J. (2016). Drought stress limits the geographic ranges of 741 two tree species via different physiological mechanisms. Global Change Biology, 22(3), 1029–1045. https://doi.org/10.1111/gcb.13148 742 743 Austin, M. W., Smith, A. B., Olsen, K. M., Hoch, P. C., Krakos, K. N., Schmocker, S. P., & 744 Miller-Struttmann, N. E. (2024). Climate change increases flowering duration, driving 745 phenological reassembly and elevated co-flowering richness. New Phytologist, 243(6), 746 2486–2500. https://doi.org/10.1111/nph.19994 747 Barbet-Massin, M., Jiguet, F., Albert, C. H., & Thuiller, W. (2012). Selecting pseudo-absences 748 for species distribution models: How, where and how many? Methods in Ecology and 749 Evolution, 3(2), 327–338. https://doi.org/10.1111/j.2041-210X.2011.00172.x 750 Barnes, P. W., & Harrison, A. T. (1982). Species distribution and community organization in a 751 Nebraska Sandhills mixed prairie as influenced by plant/soil-water relationships. 752 Oecologia, 52(2), 192–201. https://doi.org/10.1007/BF00363836 753 Belitz, M. W., Larsen, E. A., Shirey, V., Li, D., & Guralnick, R. P. (2023). Phenological research 754 based on natural history collections: Practical guidelines and a lepidopteran case study. 755 Functional Ecology, 37(2), 234–247. https://doi.org/10.1111/1365-2435.14173

- 756 Berdugo, M., Delgado-Baquerizo, M., Soliveres, S., Hernández-Clemente, R., Zhao, Y., Gaitán,
- J. J., Gross, N., Saiz, H., Maire, V., Lehmann, A., Rillig, M. C., Solé, R. V., & Maestre,
- F. T. (2020). Global ecosystem thresholds driven by aridity. *Science*, 367(6479), 787–
- 759 790. https://doi.org/10.1126/science.aay5958
- 760 Bray, J. R., & Curtis, J. T. (1957). An Ordination of the Upland Forest Communities of Southern
- 761 Wisconsin. *Ecological Monographs*, 27(4), 326–349. https://doi.org/10.2307/1942268
- CaraDonna, P. J., Iler, A. M., & Inouye, D. W. (2014). Shifts in flowering phenology reshape a
- subalpine plant community. Proceedings of the National Academy of Sciences, 111(13),
- 764 4916–4921. https://doi.org/10.1073/pnas.1323073111
- 765 Chase, J. M., Leibold, M. A., Downing, A. L., & Shurin, J. B. (2000). The Effects of
- Productivity, Herbivory, and Plant Species Turnover in Grassland Food Webs. *Ecology*,
- 767 81(9), 2485–2497. https://doi.org/10.1890/0012-
- 768 9658(2000)081%255B2485:TEOPHA%255D2.0.CO;2
- 769 Chen, Y., Collins, S. L., Zhao, Y., Zhang, T., Yang, X., An, H., Hu, G., Xin, C., Zhou, J., Sheng,
- 770 X., He, M., Zhang, P., Guo, Z., Zhang, H., Li, L., & Ma, M. (2023). Warming reduced
- flowering synchrony and extended community flowering season in an alpine meadow on
- the Tibetan Plateau. *Ecology*, 104(1), e3862. https://doi.org/10.1002/ecy.3862
- 773 Cleland, E. E., Chuine, I., Menzel, A., Mooney, H. A., & Schwartz, M. D. (2007). Shifting plant
- phenology in response to global change. *Trends in Ecology & Evolution*, 22(7), 357–365.
- 775 https://doi.org/10.1016/j.tree.2007.04.003
- 776 Cleland, E. E., Collins, S. L., Dickson, T. L., Farrer, E. C., Gross, K. L., Gherardi, L. A., Hallett,
- L. M., Hobbs, R. J., Hsu, J. S., Turnbull, L., & Suding, K. N. (2013). Sensitivity of

- grassland plant community composition to spatial vs. Temporal variation in precipitation.
- 779 *Ecology*, 94(8), 1687–1696. https://doi.org/10.1890/12-1006.1
- Cutler, D. R., Edwards Jr., T. C., Beard, K. H., Cutler, A., Hess, K. T., Gibson, J., & Lawler, J. J.
- 781 (2007). Random Forests for Classification in Ecology. *Ecology*, 88(11), 2783–2792.
- 782 https://doi.org/10.1890/07-0539.1
- 783 Daru, B. H. (2024). Predicting undetected native vascular plant diversity at a global scale.
- *Proceedings of the National Academy of Sciences*, 121(34), e2319989121.
- 785 https://doi.org/10.1073/pnas.2319989121
- 786 Elzinga, J. A., Atlan, A., Biere, A., Gigord, L., Weis, A. E., & Bernasconi, G. (2007). Time after
- time: Flowering phenology and biotic interactions. *Trends in Ecology & Evolution*, 22(8),
- 788 432–439. https://doi.org/10.1016/j.tree.2007.05.006
- 789 Epstein, H. e., Lauenroth, W. k., Burke, I. c., & Coffin, D. p. (1996). Ecological responses of
- dominant grasses along two climatic gradients in the Great Plains of the United States.
- 791 *Journal of Vegetation Science*, 7(6), 777–788. https://doi.org/10.2307/3236456
- 792 Ettinger, A. K. (2020). Winter temperatures predominate in spring phenological responses to
- 793 warming. *Nature Climate Change*, 10.
- Feeley, K. J., & Silman, M. R. (2010). Land-use and climate change effects on population size
- and extinction risk of Andean plants. *Global Change Biology*, 16(12), 3215–3222.
- 796 https://doi.org/10.1111/j.1365-2486.2010.02197.x
- 797 Fründ, J., Linsenmair, K. E., & Blüthgen, N. (2010). Pollinator diversity and specialization in
- relation to flower diversity. Oikos, 119(10), 1581–1590. https://doi.org/10.1111/j.1600-
- 799 0706.2010.18450.x

800	Fu, Y. H., Zhao, H., Piao, S., Peaucelle, M., Peng, S., Zhou, G., Ciais, P., Huang, M., Menzel,
801	A., Peñuelas, J., Song, Y., Vitasse, Y., Zeng, Z., & Janssens, I. A. (2015). Declining
802	global warming effects on the phenology of spring leaf unfolding. Nature, 526(7571),
803	104-107. https://doi.org/10.1038/nature15402
804	Gamble, D. E., & Mazer, S. J. (2022). Spatial uncertainty in herbarium data: Simulated
805	displacement but not error distance alters estimates of phenological sensitivity to climate
806	in a widespread California wildflower. Ecography, 2022(10), e06107.
807	https://doi.org/10.1111/ecog.06107
808	Godoy, O., Richardson, D. M., Valladares, F., & Castro-Díez, P. (2009). Flowering phenology of
809	invasive alien plant species compared with native species in three Mediterranean-type
810	ecosystems. Annals of Botany, 103(3), 485-494. https://doi.org/10.1093/aob/mcn232
811	Guo, J., Ma, Q., Xu, H., Luo, Y., He, D., Wang, F., Wu, J., Fu, Y. H., Liu, J., Zhang, R., & Chen,
812	L. (2023). Meta-analytic and experimental evidence that warmer climate leads to shift
813	from advanced to delayed spring phenology. Agricultural and Forest Meteorology, 342,
814	109721. https://doi.org/10.1016/j.agrformet.2023.109721
815	Huntley, B. (1991). How Plants Respond to Climate Change: Migration Rates, Individualism and
816	the Consequences for Plant Communities. Annals of Botany, 67(supp1), 15-22.
817	https://doi.org/10.1093/oxfordjournals.aob.a088205
818	Jon Dewitz. (2024). National Land Cover Database (NLCD) 2019 Products (ver. 3.0, February
819	2024) [Dataset]. U.S. Geological Survey. https://doi.org/10.5066/P9KZCM54
820	Kartesz, J. T. (2024). The Biota of North America Program (BONAP). North American Plant
821	Atlas. (Http://Www.Bonap.Net/Tdc). Chapel Hill, N.C. [Maps Generated from Kartesz,

822	J.T. 2015. Floristic Synthesis of North America, Version 1.0. Biota of North America
823	Program (BONAP).
824	Kelly, A. E., & Goulden, M. L. (2008). Rapid shifts in plant distribution with recent climate
825	change. Proceedings of the National Academy of Sciences, 105(33), 11823-11826.
826	https://doi.org/10.1073/pnas.0802891105
827	Koenker, R., Chernozhukov, V., He, X., & Peng, L. (Eds.). (2017). Handbook of Quantile
828	Regression. Chapman and Hall/CRC. https://doi.org/10.1201/9781315120256
829	Li, D., Barve, N., Brenskelle, L., Earl, K., Barve, V., Belitz, M. W., Doby, J., Hantak, M. M.,
830	Oswald, J. A., Stucky, B. J., Walters, M., & Guralnick, R. P. (2021). Climate,
831	urbanization, and species traits interactively drive flowering duration. Global Change
832	Biology, 27(4), 892–903. https://doi.org/10.1111/gcb.15461
833	Liaw, A., & Wiener, M. (2002). Classification and Regression by randomForest. R News, 2.
834	MacDougall, A. S., Esch, E., Chen, Q., Carroll, O., Bonner, C., Ohlert, T., Siewert, M., Sulik, J.,
835	Schweiger, A. K., Borer, E. T., Naidu, D., Bagchi, S., Hautier, Y., Wilfahrt, P., Larson,
836	K., Olofsson, J., Cleland, E., Muthukrishnan, R., O'Halloran, L., Seabloom, E. W.
837	(2024). Widening global variability in grassland biomass since the 1980s. Nature
838	Ecology & Evolution, 1–12. https://doi.org/10.1038/s41559-024-02500-x
839	Omernik, J. M. (1987). Ecoregions of the Conterminous United States. Annals of the Association
840	of American Geographers, 77(1), 118–125. https://doi.org/10.1111/j.1467-
841	8306.1987.tb00149.x
842	Park, D. S., Breckheimer, I., Williams, A. C., Law, E., Ellison, A. M., & Davis, C. C. (2019).
843	Herbarium specimens reveal substantial and unexpected variation in phenological
844	sensitivity across the eastern United States. Philosophical Transactions of the Royal

845 Society B: Biological Sciences, 374(1763), 20170394. 846 https://doi.org/10.1098/rstb.2017.0394 Park, I., Mazer, S., Ellison, A. E., Davis, C., Record, S., & Ramirez-Parada, T. (2023). 847 848 Herbarium-Derived Phenological Data in North America (Version 7, p. 23165279 bytes) 849 [Dataset]. Dryad. https://doi.org/10.25349/D9WP6S 850 Park, I. W., & Mazer, S. J. (2018). Overlooked climate parameters best predict flowering onset: 851 Assessing phenological models using the elastic net. Global Change Biology, 24(12), 5972–5984. https://doi.org/10.1111/gcb.14447 852 853 Park, I. W., Ramirez-Parada, T., Record, S., Davis, C., Ellison, A. M., & Mazer, S. J. (2024). 854 Herbarium data accurately predict the timing and duration of population-level flowering 855 displays. *Ecography*, e06961. https://doi.org/10.1111/ecog.06961 856 Parmesan, C., & Hanley, M. E. (2015). Plants and climate change: Complexities and surprises. 857 Annals of Botany, 116(6), 849–864. https://doi.org/10.1093/aob/mcv169 858 Potts, S. G., Vulliamy, B., Dafni, A., Ne'eman, G., & Willmer, P. (2003). Linking bees and 859 flowers: How do floral communities structure pollinator communities? *Ecology*, 84(10), 860 2628–2642. https://doi.org/10.1890/02-0136 861 Ramirez-Parada, T. H., Park, I. W., Record, S., Davis, C. C., Ellison, A. M., & Mazer, S. J. 862 (2024). Plasticity and not adaptation is the primary source of temperature-mediated 863 variation in flowering phenology in North America. Nature Ecology & Evolution, 8(3), 864 467–476. https://doi.org/10.1038/s41559-023-02304-5 Ramirez-Parada, T. H., Park, I. W., Record, S., Davis, C. C., & Mazer, S. J. (2025). Scaling 865 866 flowering onset and duration responses among species predicts phenological community

867	reassembly under warming. Ecosphere, 16(3), e70070.
868	https://doi.org/10.1002/ecs2.70070
869	Renner, S. S., & Zohner, C. M. (2018). Climate Change and Phenological Mismatch in Trophic
870	Interactions Among Plants, Insects, and Vertebrates. Annual Review of Ecology,
871	Evolution, and Systematics, 49(Volume 49, 2018), 165–182.
872	https://doi.org/10.1146/annurev-ecolsys-110617-062535
873	Riahi, K., van Vuuren, D. P., Kriegler, E., Edmonds, J., O'Neill, B. C., Fujimori, S., Bauer, N.,
874	Calvin, K., Dellink, R., Fricko, O., Lutz, W., Popp, A., Cuaresma, J. C., Kc, S.,
875	Leimbach, M., Jiang, L., Kram, T., Rao, S., Emmerling, J., Tavoni, M. (2017). The
876	Shared Socioeconomic Pathways and their energy, land use, and greenhouse gas
877	emissions implications: An overview. Global Environmental Change, 42, 153-168.
878	https://doi.org/10.1016/j.gloenvcha.2016.05.009
879	Rogelj, J., Meinshausen, M., & Knutti, R. (2012). Global warming under old and new scenarios
880	using IPCC climate sensitivity range estimates. Nature Climate Change, 2(4), 248–253.
881	https://doi.org/10.1038/nclimate1385
882	Roulston, T. H., & Goodell, K. (2011). The Role of Resources and Risks in Regulating Wild Bee
883	Populations. Annual Review of Entomology, 56(Volume 56, 2011), 293–312.
884	https://doi.org/10.1146/annurev-ento-120709-144802
885	Rutishauser, T., Luterbacher, J., Defila, C., Frank, D., & Wanner, H. (2008). Swiss spring plant
886	phenology 2007: Extremes, a multi-century perspective, and changes in temperature
887	sensitivity. Geophysical Research Letters, 35(5), 2007GL032545.
888	https://doi.org/10.1029/2007GL032545

889	Schenk, M., Krauss, J., & Holzschuh, A. (2018). Desynchronizations in bee-plant interactions
890	cause severe fitness losses in solitary bees. Journal of Animal Ecology, 87(1), 139–149.
891	https://doi.org/10.1111/1365-2656.12694
892	Seager, R., Feldman, J., Lis, N., Ting, M., Williams, A. P., Nakamura, J., Liu, H., & Henderson,
893	N. (2018). Whither the 100th Meridian? The Once and Future Physical and Human
894	Geography of America's Arid-Humid Divide. Part II: The Meridian Moves East. Earth
895	Interactions, 22(5), 1-24. https://doi.org/10.1175/EI-D-17-0012.1
896	Sohl, T. L., Sayler, K. L., Bouchard, M. A., Reker, R. R., Friesz, A. M., Bennett, S. L., Sleeter,
897	B. M., Sleeter, R. R., Wilson, T., Soulard, C., Knuppe, M., & Van Hofwegen, T. (2014).
898	Spatially explicit modeling of 1992–2100 land cover and forest stand age for the
899	conterminous United States. Ecological Applications, 24(5), 1015-1036.
900	https://doi.org/10.1890/13-1245.1
901	Sohl, T., Reker, R., Bouchard, M., Sayler, K., Dornbierer, J., Wika, S., Quenzer, R., & Friesz, A.
902	(2016). Modeled historical land use and land cover for the conterminous United States.
903	Journal of Land Use Science, 11(4), 476–499.
904	https://doi.org/10.1080/1747423X.2016.1147619
905	Sponsler, D., Iverson, A., & Steffan-Dewenter, I. (2023). Pollinator competition and the structure
906	of floral resources. <i>Ecography</i> , 2023(9), e06651. https://doi.org/10.1111/ecog.06651
907	Theobald, E. J., Breckheimer, I., & HilleRisLambers, J. (2017). Climate drives phenological
908	reassembly of a mountain wildflower meadow community. <i>Ecology</i> , 98(11), 2799–2812.
909	https://doi.org/10.1002/ecy.1996

910	Valavi, R., Guillera-Arroita, G., Lahoz-Monfort, J. J., & Elith, J. (2022). Predictive performance
911	of presence-only species distribution models: A benchmark study with reproducible code.
912	Ecological Monographs, 92(1), e01486. https://doi.org/10.1002/ecm.1486
913	Walker, K. (2016). tigris: An R Package to Access and Work with Geographic Data from the US
914	Census Bureau. The R Journal. https://digitalcommons.unl.edu/r-journal/491
915	Wolf, A. A., Zavaleta, E. S., & Selmants, P. C. (2017). Flowering phenology shifts in response to
916	biodiversity loss. Proceedings of the National Academy of Sciences, 114(13), 3463–3468.
917	https://doi.org/10.1073/pnas.1608357114
918	Woodcock, B. A., Garratt, M. P. D., Powney, G. D., Shaw, R. F., Osborne, J. L., Soroka, J.,
919	Lindström, S. a. M., Stanley, D., Ouvrard, P., Edwards, M. E., Jauker, F., McCracken, M.
920	E., Zou, Y., Potts, S. G., Rundlöf, M., Noriega, J. A., Greenop, A., Smith, H. G.,
921	Bommarco, R., Pywell, R. F. (2019). Meta-analysis reveals that pollinator functional
922	diversity and abundance enhance crop pollination and yield. Nature Communications,
923	10(1), 1481. https://doi.org/10.1038/s41467-019-09393-6
924	Zettlemoyer, M. A., Schultheis, E. H., & Lau, J. A. (2019). Phenology in a warming world:
925	Differences between native and non-native plant species. Ecology Letters, 22(8), 1253-
926	1263. https://doi.org/10.1111/ele.13290
927	Zhou, Z., Zhang, K., Sun, Z., Liu, Y., Zhang, Y., Lei, L., Li, Y., Wang, D., Hu, M., Wang, S.,
928	Lu, Q., Cui, Y., Zhong, M., Han, S., & Miao, Y. (2022). Lengthened flowering season
929	under climate warming: Evidence from manipulative experiments. Agricultural and
930	Forest Meteorology, 312, 108713. https://doi.org/10.1016/j.agrformet.2021.108713
931	
932	
933	

Supplemental Information for: Shifts in phenology and species ranges synergistically alter the timing and species composition of the flowering season
 Authors: Tadeo H. Ramirez-Parada, Isaac W. Park, Shijia Peng, Misako Nishino, John T. Kartesz, Sydne Record, Charles C. Davis, Susan J. Mazer.
 Contact: Tadeo H. Ramirez-Parada, tadeoramirezp@gmail.com

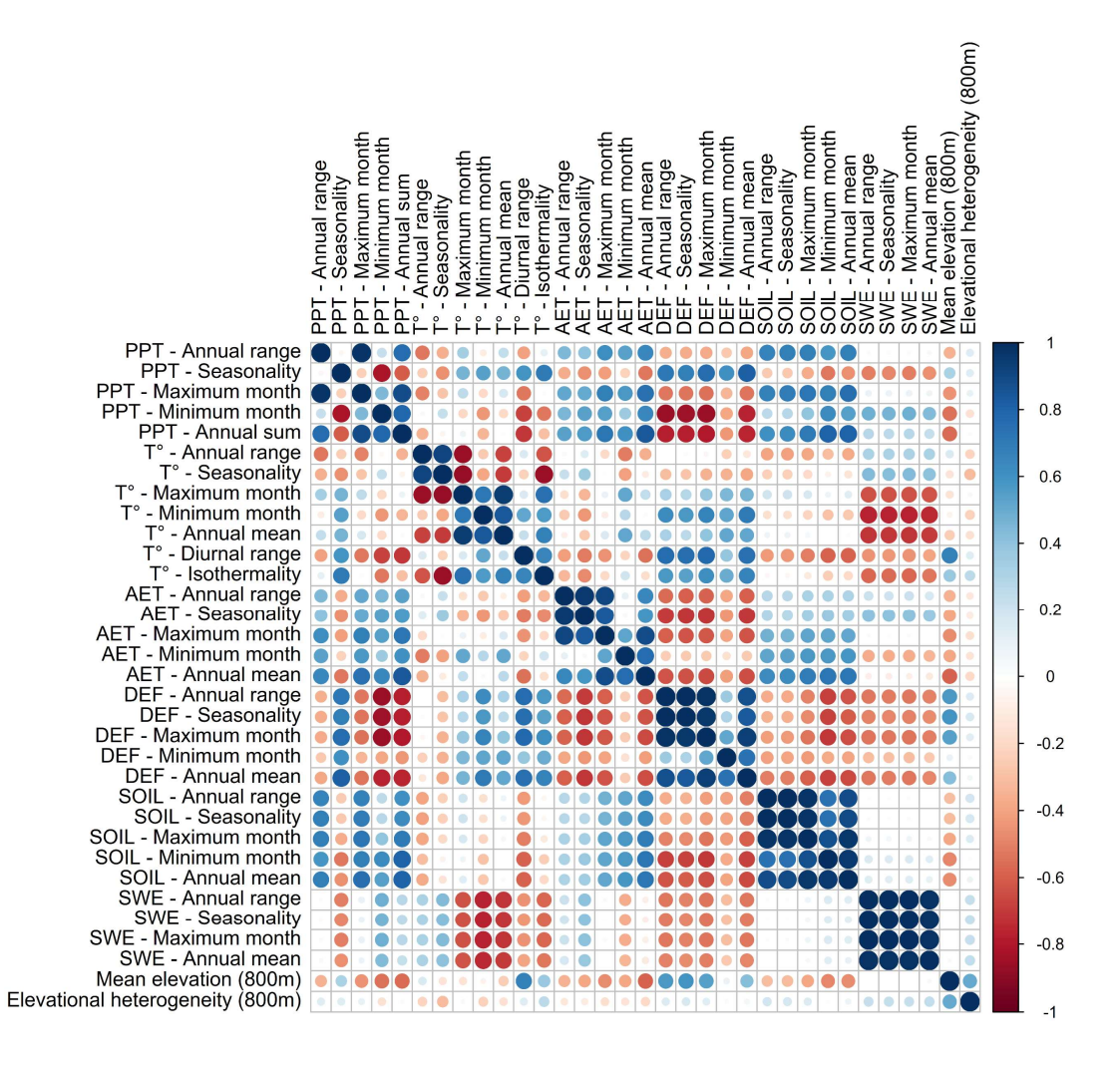


**Figure S1**—Correlations among 2004-2023 normals for 31 climatic variables, mean elevation, and elevation heterogeneity across 4km resolution grid cells throughout the conterminous United States. Climate variables include annual sums or means, maximum monthly values, minimum monthly values, annual monthly range, and seasonality for precipitation (PPT), temperature (T°), actual evapotransporation (AET), climate water deficit (DEF), soil moisture (SOIL), and snowwater equivalent (SWE). Variables for T° also include approximate mean daily range, and isothermality. Seasonality for precipitation was calculated proportionally to the mean cumulative annual precipitation in each site.

	PC1 (1.9, 43%)	PC2 (1.7, 43%)	PC3 (1.3, 9%)	PC4 (1.2, 6%)	PC5 (1.1, 5%)
PPT - Annual range	-0.15	-0.21	0.14	-0.05	0.22
PPT - Seasonality	0.20	-0.10	0.10	-0.11	0.18
PPT - Monthly maximum	-0.19	-0.18	0.10	-0.09	0.16
PPT - Monthly minimum	-0.22	0.02	-0.11	-0.17	-0.20
PPT - Annual sum	-0.23	-0.12	0.01	-0.10	-0.03
T° - Annual range	0.01	0.27	-0.20	0.29	0.08
T° - Seasonality	-0.07	0.26	-0.25	0.23	0.00
T° - Monthly minimum	0.08	-0.30	0.04	-0.22	-0.07
T° - Monthly maximum	0.16	-0.20	-0.20	-0.02	-0.03
T° - Annual mean	0.09	-0.29	-0.12	-0.22	-0.05
T° - Diurnal range	0.21	-0.01	0.04	0.10	0.19
T° - Isothermality	0.16	-0.21	0.18	-0.16	0.12
AET - Annual range	-0.17	-0.02	-0.19	-0.11	0.49
AET - Seasonality	-0.20	0.04	-0.15	-0.12	0.42
AET - Monthly maximum	-0.19	-0.13	-0.19	-0.07	0.35
AET- Monthly minimum	-0.09	-0.26	-0.06	0.06	-0.15
AET - Annual mean	-0.20	-0.19	-0.16	0.02	0.07
DEF - Annual range	0.24	-0.04	0.08	0.15	0.11
DEF - Seasonality	0.24	-0.03	0.10	0.19	0.09
DEF - Monthly maximum	0.25	-0.05	0.07	0.06	0.07
DEF- Monthly minimum	0.16	-0.06	-0.02	-0.38	-0.16
DEF - Annual mean	0.25	-0.06	0.03	-0.11	-0.02

SOIL - Annual range	-0.16	-0.18	0.21	0.27	0.01
SOIL - Seasonality	-0.16	-0.18	0.21	0.26	-0.01
SOIL - Monthly maximum	-0.19	-0.17	0.18	0.23	-0.06
SOIL - Monthly minimum	-0.21	-0.13	0.08	0.11	-0.19
SOIL - Annual mean	-0.21	-0.16	0.14	0.16	-0.15
SWE - Annual range	-0.14	0.24	0.21	-0.19	-0.02
SWE - Seasonality	-0.14	0.24	0.21	-0.20	-0.02
SWE - Monthly maximum	-0.14	0.24	0.21	-0.19	-0.02
SWE – Annual mean	-0.13	0.24	0.22	-0.21	-0.02
Mean Elevation (800m)	0.14	0.10	0.28	0.13	0.25
Elevational heterogeneity (800m)	0.01	0.01	0.46	-0.02	0.19

**Table S2**—Loadings from a principal component analysis (PCA) of 2004-2023 normals for 31 climatic variables, mean elevation, and elevation heterogeneity across 4km resolution grid cells throughout the conterminous United States. Loadings are reported for the 5 principal components (PCs) explaining more variance than any input variable in the data. Highlighted values in each column correspond to the 5 input variables with the highest loadings on each PC. Values next to each PC's name in the column headings indicate its eigenvalue and variance explained.

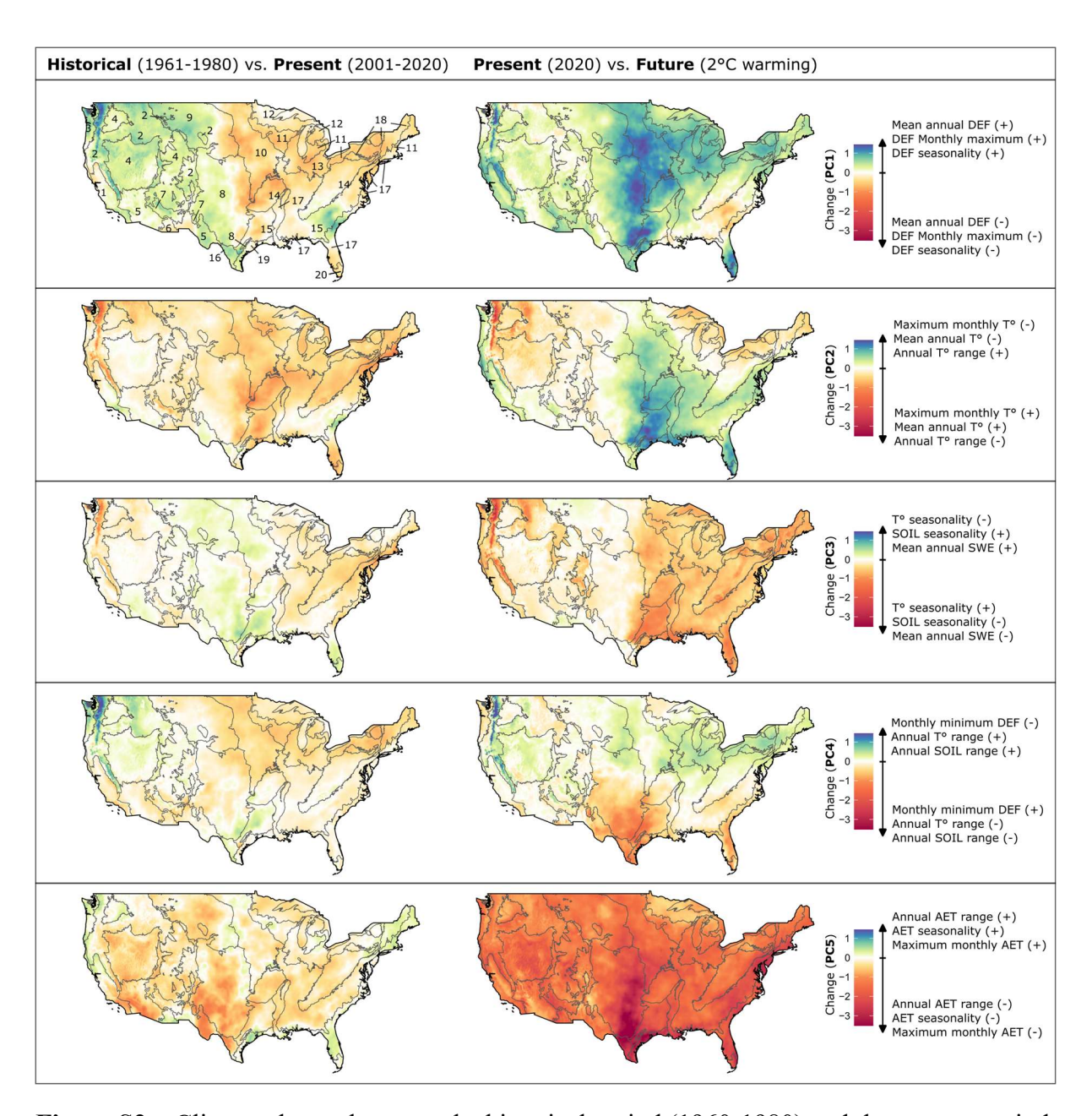


Figure S2—Climate change between the historical period (1960-1980) and the present period (2001-2020), and between the present period and projected conditions under a scenario of 2°C warming above pre-industrial levels. Climate change is shown as the difference in the 5 principal components summarizing 31 climatic variables, as well as mean elevation and elevational heterogeneity within 4km grid cells throughout the conterminous United States (see 'Methods' section of the main text) between periods. The variables listed in each legend correspond to those with the greatest loadings for each PC. Positive and negative signs next to each variable indicate whether positive or negative values in the color scale are associated to increases or decreases between periods. Subdivisions labeled 1-18 represent level II ecoregions. 1) Mediterranean California, 2) Western Cordillera, 3) Marine West Coast Forest, 4) Cold Deserts, 5) Warm Deserts, 6) Western Sierra Madre Piedmont, 7) Upper Gila Mountains, 8) South-Central Semi-

arid Prairies, 9) West-Central Semi-arid Prairies, 10) Temperate Prairies, 11) Mixed Wood Plains, 12) Mixed Wood Shield, 13) Central USA Plains, 14) Ozark, Ouachita-Appalachian Forests, 15) Southeastern USA Plains, 16) Mississippi Alluvial and Southeast USA Coastal Plain, 17) Atlantic Highlands, 18) Texas-Louisiana Coastal Plain, 19) Tamaulipas-Texas Semi-arid Plains, 20) Everglades.

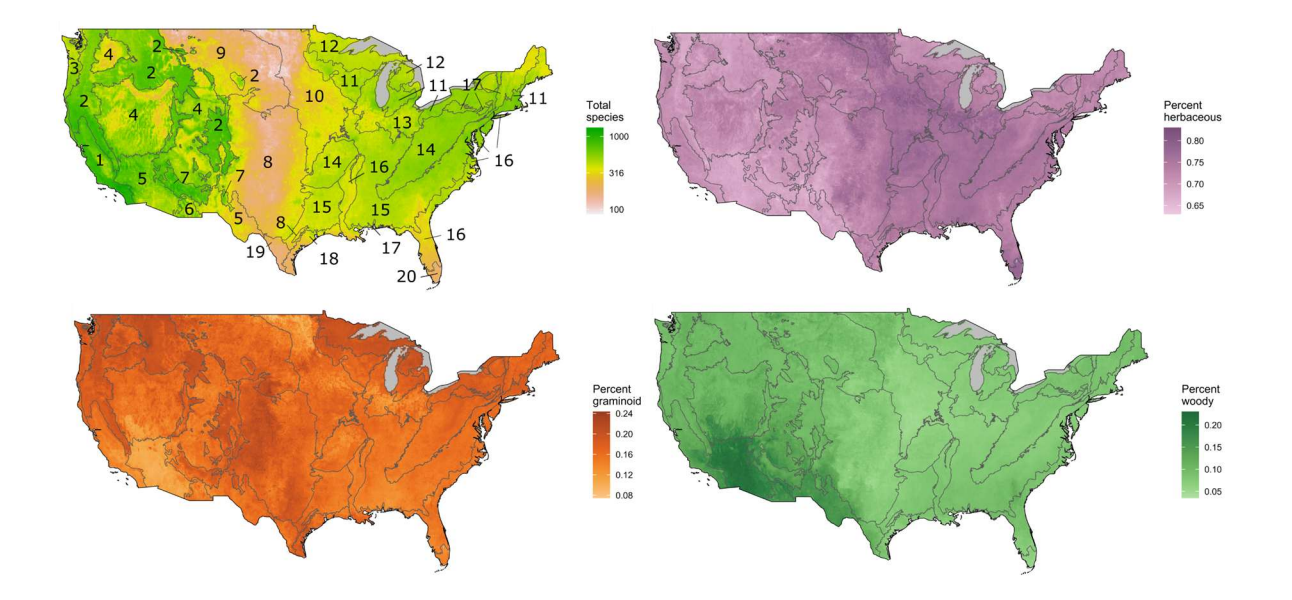
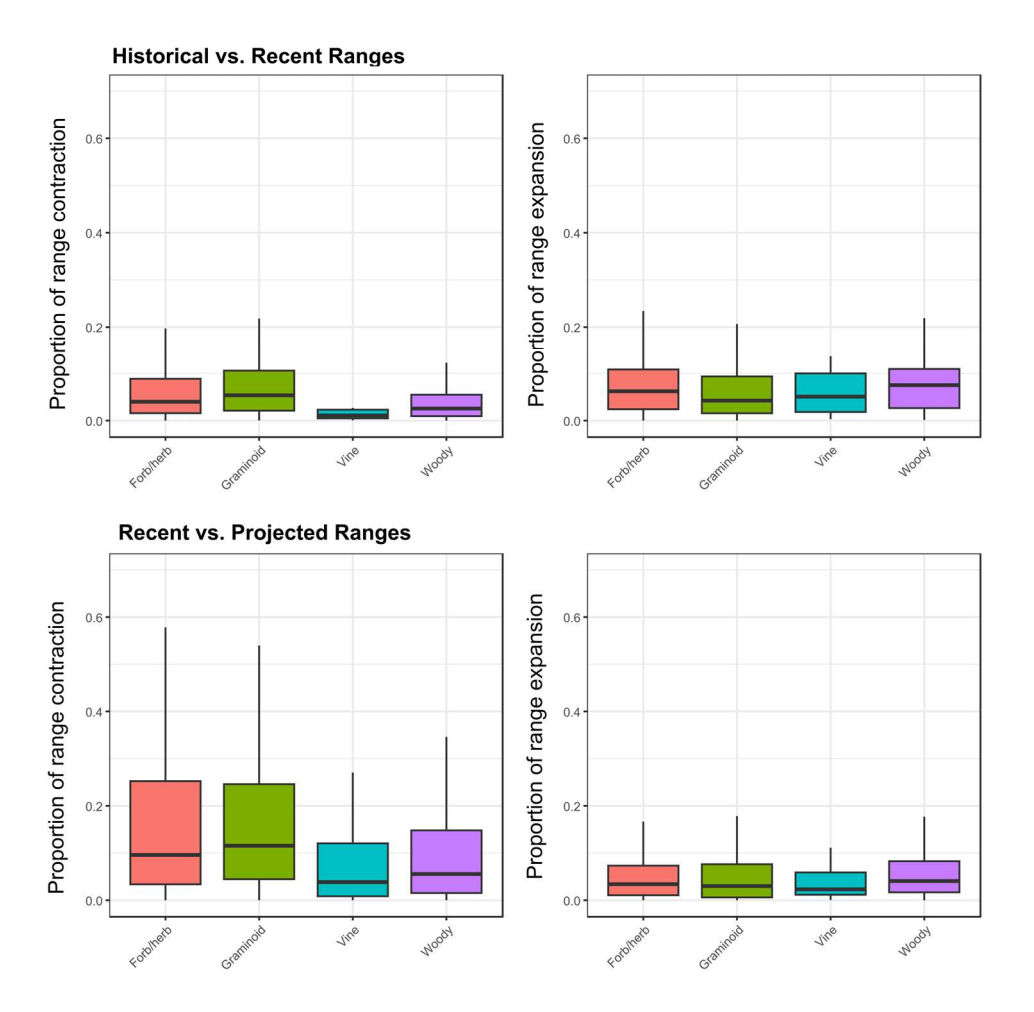
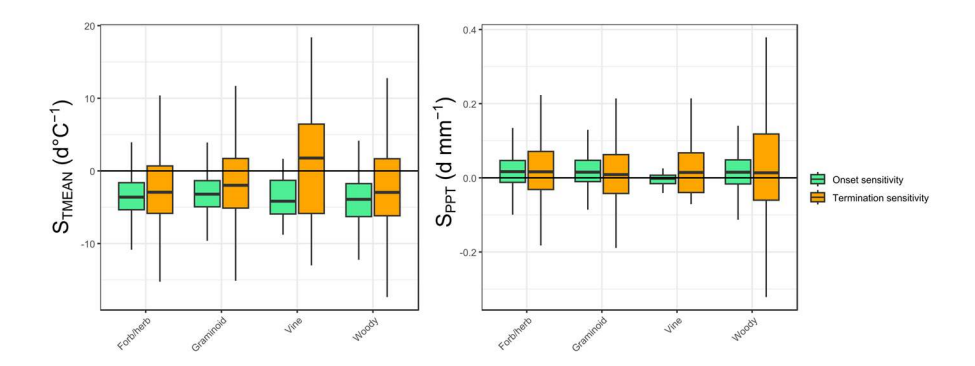


Figure S3—Predicted species richness (from a total of 2,837 species) within 12km resolution grid cells across the conterminous United States estimated for the 2001-2020 period, and the percent that have herbaceous, graminoid, or woody growth habit. Subdivisions labeled 1-18 represent level II ecoregions. 1) Mediterranean California, 2) Western Cordillera, 3) Marine West Coast Forest, 4) Cold Deserts, 5) Warm Deserts, 6) Western Sierra Madre Piedmont, 7) Upper Gila Mountains, 8) South-Central Semi-arid Prairies, 9) West-Central Semi-arid Prairies, 10) Temperate Prairies, 11) Mixed Wood Plains, 12) Mixed Wood Shield, 13) Central USA Plains, 14) Ozark, Ouachita-Appalachian Forests, 15) Southeastern USA Plains, 16) Mississippi Alluvial and Southeast USA Coastal Plain, 17) Atlantic Highlands, 18) Texas-Louisiana Coastal Plain, 19) Tamaulipas-Texas Semi-arid Plains, 20) Everglades.



**Figure S4**—Variation among growth forms in range expansion and contraction between historical (1961-1980) and recent (2001-2020) environmental conditions, or between recent and projected (2°C, B1 SRES scenario) environmental conditions. Proportion of range contraction was calculated as the number of cells predicted to be occupied by a given species in one period but not the next, divided by the number of cells occupied by the species in the previous period. Range expansions were calculated using the number of new cells predicted to be occupied by the species in the following period instead. Filled bars in the boxplot represent the 25th-75th percentile range of each metric, with solid bars corresponding to medians. The whiskers in each bar correspond to 1.5 times the interquantile distance between the 25th and 75th percentiles, an interval that encompasses approximately 95% of observations. Growth forms were obtained from the United States Department of Agriculture's (USDA) Plant List (https://plants.usda.gov/). The number of species for each growth form were 2,102 for herbs, 336 for graminoids, 378 for woody species, and 15 for vines (with 6 species missing from the Plant List).



**Figure S5**—Differences among growth forms in the sensitivity of flowering onset and termination to interannual variation in temperature and precipitation (see 'Methods' section of the main text). Filled bars in the boxplot represent the 25<sup>th</sup>-75<sup>th</sup> percentile range of each metric, with the solid horizontal bars corresponding to medians. The whisker in each bar correspond to 1.5 times the interquantile distance between the 25<sup>th</sup> and 75<sup>th</sup> percentiles, an interval that encompasses approximately 95% of observations. Growth forms were obtained from the United States Department of Agriculture's (USDA) Plant List (https://plants.usda.gov/). The number of species for each growth form were 2,102 for herbs, 336 for graminoids, 378 for woody species, and 15 for vines (with 6 species missing from the Plant List).

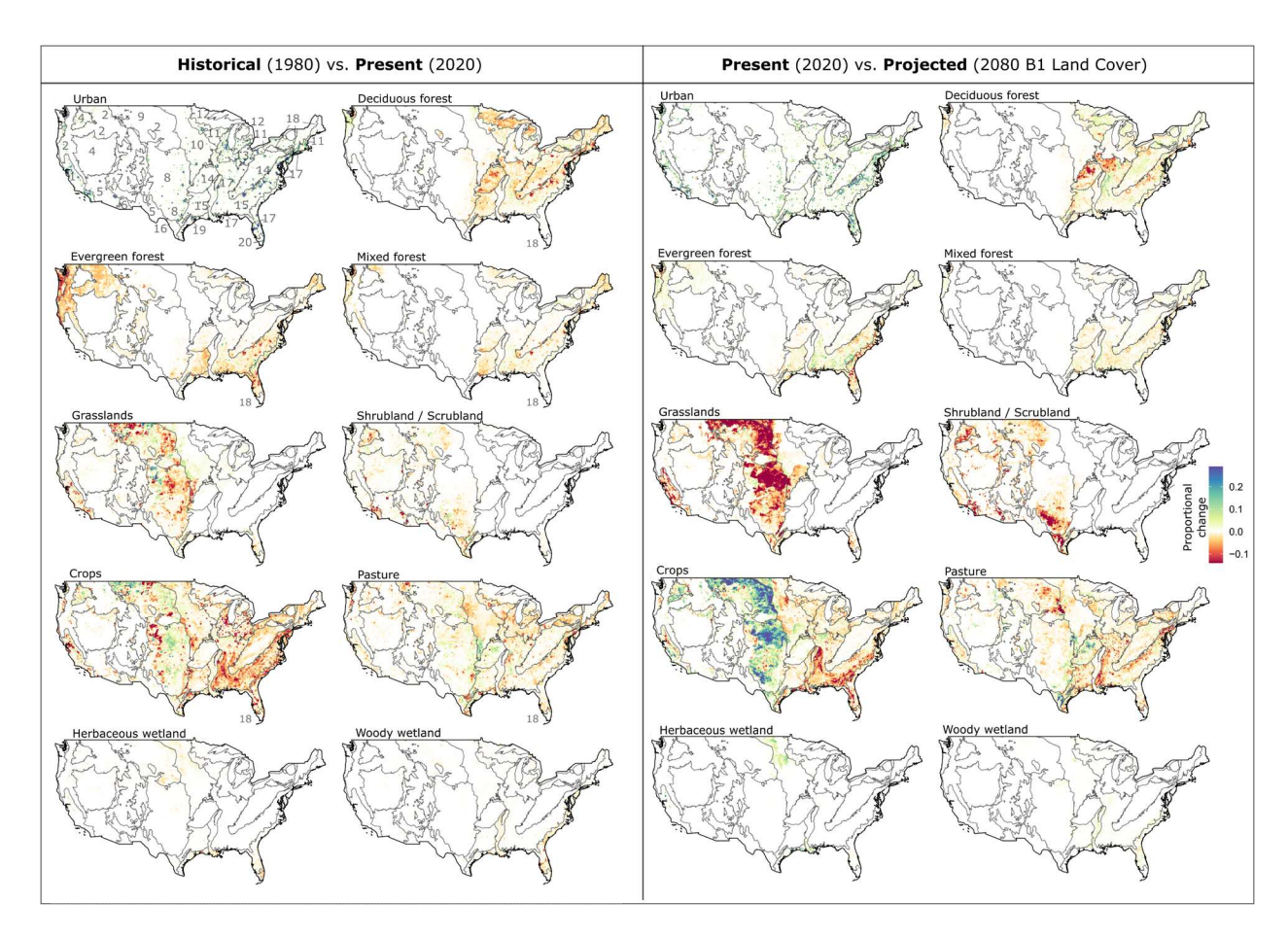


Figure S6—Change in land cover between 1980 and 2020, and between 2020 and 2080 under SRES B1 scenario of land use and land cover change. Each panel shows changes in the proportion of 250m cells of the focal class found within each 750m resolution grid cell across the conterminous United States (CONUS). Subdivisions labeled 1-18 represent level II ecoregions. 1) Mediterranean California, 2) Western Cordillera, 3) Marine West Coast Forest, 4) Cold Deserts, 5) Warm Deserts, 6) Western Sierra Madre Piedmont, 7) Upper Gila Mountains, 8) South-Central Semi-arid Prairies, 9) West-Central Semi-arid Prairies, 10) Temperate Prairies, 11) Mixed Wood Plains, 12) Mixed Wood Shield, 13) Central USA Plains, 14) Ozark, Ouachita-Appalachian Forests, 15) Southeastern USA Plains, 16) Mississippi Alluvial and Southeast USA Coastal Plain, 17) Atlantic Highlands, 18) Texas-Louisiana Coastal Plain, 19) Tamaulipas-Texas Semi-arid Plains, 20) Everglades.